Leading-logarithmic approximation by one-loop renormalization group within Matsubara formalism

Jan Diekmann◉ and Severin G. Jakobs◉

Institut für Theorie der Statistischen Physik, RWTH Aachen University, 52056 Aachen, Germany
and JARA–Fundamentals of Future Information Technology, 52056 Aachen, Germany

We demonstrate how to devise a Matsubara-formalism-based one-loop approximation to the flow of the functional renormalization group (FRG) that reproduces identically the leading-logarithmic parquet approximation. This construction of a controlled fermionic FRG approximation in a regime not accessible by perturbation theory generalizes a previous study from the real-time zero-temperature formalism to the Matsubara formalism and thus to the *de facto* standard framework used for condensed-matter FRG studies. Our investigation is based on a simple model for the absorption of x rays in metals. It is a core part of our construction to exploit that in a suitable leading-logarithmic approximation the values of the particle-hole susceptibility on the real- and on the imaginary-frequency axes are identical.

I. INTRODUCTION

Consider the function $x \mapsto x^{f(g)}$ in which the exponent $f(g) = a_1 g + a_2 g^2 + \cdots$ has a well-behaved power-series expansion without constant term $a_0 g^0$. Then

$$x^{f(g)} = \exp[(a_1 g + a_2 g^2 + \cdots) \ln x] \quad (1)$$

$$= x^{a_1 g} \exp[(a_2 g^2 + \cdots) \ln x] \quad (2)$$

$$\approx x^{a_1 g}. \quad (3)$$

This approximation is good if $g \ll 1$ is so small that $g^2 \ln x \ll 1$. The approximation allows even for large $\ln x$, and for $g \ln x$ that is not small. In a clearly defined regime of x the approximation is thus *a priori* known to be good, and it is known to become better with decreasing g.

Such a *controlled* approximation is just the result of the leading-logarithmic parquet approximation to certain many-body models in condensed-matter theory whose perturbation theory suffers from logarithmic divergencies. In the above example, the failure of perturbation theory becomes visible when one expands $x^{f(g)}$ up to first (or higher) order in g (which plays the role of the coupling constant),

$$x^{f(g)} \approx 1 + a_1 g \ln x. \quad (4)$$

This approximation is indeed not appropriate when $g \ln x$ is not small. Among the most renowned applications of the leading-logarithmic parquet approximation in condensed-matter physics are those to the Kondo model [1], to the one-dimensional interacting Fermi gas [2], and to x-ray absorption in metals [3] from which the above example is taken. These models of interacting zero- and one-dimensional Fermi systems share the pattern in which logarithmic divergencies arise in diagrammatic perturbation theory: the dominant, "leading" terms are contained in the so-called parquet diagrams.

In Ref. [4] we demonstrated a close relation between the leading-logarithmic parquet approximation and another, at first sight separate, approximation: the one-loop flow of the functional renormalization group (FRG). We substantiated for a model of x-ray absorption that a suitably crafted one-loop FRG approximation is identical on a detailed technical level to the leading-logarithmic parquet approximation. While this complete identity of the two methods is a unique observation, it has been known for a long time that renormalization group (RG) approaches are able to reproduce the results of leading-logarithmic parquet treatments: This can be achieved already with basic scaling techniques for the Kondo problem [5], for x-ray absorption [6], and for one-dimensional conductors [7] (see also [8]).

The FRG mentioned above is a modern formulation of the RG idea, based on generating functionals [9–13]. In this formalism, the flow equation of a suitable generating functional entails a hierarchy of flow equations for vertex functions. The RG flow of the vertex functions can also be understood from a distinctly diagrammatic point of view [14]. This allows to compare FRG approximations in detail with diagrammatic ones like the parquet approximation, as done, e.g., in Refs. [4,15–17].

The FRG is nowadays applied to a broad variety of models in condensed-matter theory, including interacting zero- and one-dimensional fermionic models for quantum dots and wires [9,18]. For some of these applications, the applied approximations are known to reproduce correctly the leading scaling behavior, which is not accessible by finite-order perturbation theory. Notable examples are the scaling of the backscattering self-energy component for Luttinger liquids with impurities [19] and the scaling of the hopping between localized level and leads for the interacting resonant level model at large bandwidth [20,21]. In these particular cases, the leading approximation to the scaling behavior follows already in the lowest-level truncation scheme and allows thus

115134-1

for a short and lucid derivation. Many applications of the fermionic FRG to quantum dot structures, however, do not focus on the idea of constructing a controlled approximation, especially if they use a higher-level truncation scheme. Instead, the arguments applied to justify approximate truncations of the FRG flow equations are often either perturbative or they are given *a posteriori* by comparing the results with those of other methods. A characteristic example for this situation is given by numerous FRG treatments [22–31] of the single-impurity Anderson model [32]. It is known that the Anderson model at small *s-d* mixing can be mapped onto the antiferromagnetic spin-$\frac{1}{2}$ Kondo model by a unitary transformation [33]; and it is known that the summation of the leading logarithms of the Kondo model provides meaningful results for the scattering amplitude at temperatures moderately above the Kondo temperature [1]. However, typical FRG treatments of the Anderson model are not concerned with identifying these leading logarithms in a suitable perturbation theory of that model in order to systematically include them into the approximation. Instead, most approaches start from integrating out the lead propagation and treating the onsite interaction as perturbation; this leads to a perturbation theory without logarithmic divergencies. The FRG approaches then typically achieve a somewhat extended range of applicability compared to second-order perturbation theory, but do not provide a reliable access to the Kondo regime [22–27,30,31]. One FRG scheme exploiting Ward identities was able to reproduce Kondo scaling but used four fit parameters for an interaction-dependent regulator [29]. And while Ref. [28] is exceptional in being based on a differently organized perturbation theory, it does not provide a systematic consideration of leading contributions. In summary, none of the cited FRG approaches to the Anderson impurity model are controlled *a priori* in the Kondo regime.

We believe that it is worthwhile to reinforce the quest for controlled FRG approximations applicable to models for quantum dots and wires, in particular for situations which require truncations beyond the one on the lowest level. Such approximations could combine the efficiency and analytic accessibility of the FRG with an *a priori* known reliability. As a first step in this program, we constructed in Ref. [4] the aforementioned one-loop FRG approximation that reproduces identically the leading-logarithmic parquet approximation for a model of x-ray absorption in metals. In that reference, we created and used a formulation of the FRG within the real-time zero-temperature ground-state formalism to be as close as possible to the parquet treatment of this model from Ref. [3]. However, most applications of the FRG to condensed-matter problems are implemented within the imaginary-time finite-temperature Matsubara formalism [9–13]. It is hence naturally our next goal to transfer our analysis of Ref. [4] to the Matsubara formalism. This transfer is realized in this paper: We show how to devise, within Matsubara formalism, a one-loop FRG approximation for the x-ray absorption problem that reproduces identically the leading-logarithmic parquet approximation.

The paper is organized as follows. In Sec. II we set up the formal framework to describe x-ray absorption in metals. We start by briefly introducing the underlying model in Sec. II A. Then we discuss in Sec. II B how the ground state of that

system depends on the energy level of the localized deep state. On this basis we can later relate the description of the model in the Matsubara formalism to the one in the real-time zero-temperature ground-state formalism. The relation between the formalisms then helps us to benefit from results of Refs. [3,4]. In Sec. II C we delineate how the linear response rate of x-ray absorption can be computed from the imaginary-time exciton propagator. This propagator in turn is accessible by fermionic diagrammatic perturbation theory in Matsubara formalism. In Sec. III we expound how we employ the Matsubara formalism at $T = 0$ with continuous Matsubara frequencies and with a specific choice of the deep-state energy. Within this formal framework we then apply a leading-logarithmic approximation to the local conduction-state propagator in Sec. IV. We show that this approximation makes the imaginary-frequency diagrammatic expressions coincide with the real-frequency ones. From that observation onwards, all further steps can be copied from our previous study in Ref. [4]. In Sec. V we relate our construction of a leading-logarithmic one-loop Matsubara FRG approximation to the observation from Ref. [16] that multiloop FRG improves the results of one-loop FRG for the model under consideration. Finally, we conclude in Sec. VI. Detailed explanations of several technical issues can be found in the Appendixes.

II. X-RAY ABSORPTION AND EXCITON PROPAGATOR

In this section we establish the formal basis underlying all later considerations. First we introduce (Sec. II A) a simple model system for x-ray absorption known from Ref. [3]. Later we identify the propagator of a local exciton as a many-body quantity that allows to determine the rate of x-ray absorption (Sec. II C). In order to relate the Matsubara exciton propagator to the one from the real-time zero-temperature formalism, a clear understanding of the ground state of the model system is required. Therefore, the ground state is studied in Sec. II B.

A. Model system

The model studied in this paper is identical to the one in our previous paper [4] and essentially taken from Ref. [3]. It is a basic model for the theoretical analysis of x-ray absorption in metals. The Hamiltonian of spinless electrons is given by

$$H = H_0 - \frac{U}{V} \sum_{kk'} a_{k'}^\dagger a_k a_d a_d^\dagger, \tag{5}$$

$$H_0 = \epsilon_d a_d^\dagger a_d + \sum_k \epsilon_k a_k^\dagger a_k. \tag{6}$$

Here, $a_d^\dagger$ creates an electron in a localized "deep" state with energy $\epsilon_d < 0$ and $a_k^\dagger$ creates an electron with momentum k in the conduction band which extends from $-\xi_0$ to $\xi_0 > 0$ with a constant density of states ρ. For simplicity, we assume the total number of momentum eigenstates in the conduction band to be even and denote it by $2N = 2\xi_0\rho$. A hole on the deep state leads to a local attractive potential for the electrons in the conduction band. The amplitude $-U < 0$ of this interaction is independent of the conduction-electron momenta; V denotes the volume of the conductor. We consider the system primarily at zero temperature and with a half-filled conduction band.

Our quantity of interest is the linear response rate $R(\nu)$ of absorption of x rays from a perturbing x-ray field with frequency ν. This field is assumed to interact with the system via an additional addend to the Hamiltonian, namely,

$$H_X(t) = e^{-i\nu t} W A^\dagger + \text{H.c.} \tag{7}$$

Here,

$$A^\dagger = \frac{1}{\sqrt{V}} \sum_k a_k^\dagger a_d \tag{8}$$

creates a local particle-hole excitation. As the electromagnetic field is not quantized, the rate of x-ray absorptions is derived from the rate of electronic transitions (compare Sec. II C).

The absorption rate is known to vanish for frequencies below some threshold ν_c, above which the leading behavior is a power-law divergence $R(\nu) \propto [\xi_0/(\nu - \nu_c)]^{2g}$ with $g = \rho U / V$ denoting the dimensionless coupling constant [3,34,35]. An expansion of $R(\nu)$ in powers of g leads to a series in powers of $g \ln[\xi_0/(\nu - \nu_c)]$. (We use units with $\hbar = 1$ and also $k_B = 1$.) Correspondingly, a treatment of this model with many-body perturbation theory leads to logarithmic divergencies; these appear in bubbles of particle-particle and particle-hole propagation. The way in which the divergencies occur is prototypical for a class of low-dimensional fermionic systems which includes the Kondo model [1] and the one-dimensional interacting Fermi gas [2,7].

B. Ground state of the system

In the subsequent sections it is necessary to understand how the ground state of the system filled with $N + 1$ particles depends on the value of ϵ_d. This is clarified in this section in which we explain that there exist two many-body states $|\Psi_0\rangle$ and $|\bar\Psi_0\rangle$ and a threshold value ϵ_{d0} such that the ground state changes from $|\Psi_0\rangle$ for $\epsilon_d < \epsilon_{d0}$ to $|\bar\Psi_0\rangle$ for $\epsilon_d > \epsilon_{d0}$. (The particular case $\epsilon_d = \epsilon_{d0}$ with a degeneracy of the ground state will not be important for us.)

Since the Hamiltonian commutes with the deep-state occupancy n_d there exists a Hilbert space basis that consists of common eigenstates of both operators: the eigenstates of H can be chosen to have either an occupied or an empty deep level. Let $|\Psi_0\rangle$ denote the energetically lowest state in the subspace with occupied deep level and let $|\bar\Psi_0\rangle$ denote the energetically lowest state in the subspace with empty deep level. Depending on ϵ_d, either $|\Psi_0\rangle$ or $|\bar\Psi_0\rangle$ has the lower energy and is thus the ground state.

We first consider $|\Psi_0\rangle$. Since H equals H_0 on the subspace with $n_d = 1$, $|\Psi_0\rangle$ is the Slater determinant type many-body state in which the deep level and the N momentum states in the lower half of the conduction band are occupied, while the states in the upper half of the conduction band are empty. The energy of this state is

$$E_0 = \epsilon_d + E_{cb} \tag{9}$$

where E_{cb} is the energy of the half-filled conduction band,

$$E_{cb} = \rho \int_{-\xi_0}^0 d\epsilon\, \epsilon = -\frac{\rho \xi_0^2}{2}. \tag{10}$$

Next we discuss $|\bar\Psi_0\rangle$. On the subspace with $n_d = 0$, the Hamiltonian H is equal to the perturbed single-particle Hamiltonian

$$\bar H_0 = \sum_{k,k'} \left(\delta_{kk'} \epsilon_k - \frac{U}{V} \right) a_{k'}^\dagger a_k. \tag{11}$$

The single-particle eigenstates of $\bar H_0$ are not the momentum states k_n but perturbed scattering states $\bar k_n$ to energies $\bar\epsilon_n$, which we sort as $\bar\epsilon_1 < \bar\epsilon_2 < \cdots < \bar\epsilon_{2N}$. To be more precise, the particular state with the lowest perturbed single-particle energy $\bar\epsilon_1 =: \bar\epsilon_b$ is a bound state resulting from the localized attractive potential generated by the deep hole. Its energy is approximately

$$\bar\epsilon_b \approx -\xi_0 (1 + 2 e^{-1/g}) \tag{12}$$

for $1 \gg g \gg 1/\ln(2\xi_0 \rho)$ (see Appendix A for more details). In the $(N + 1)$-particle state $|\bar\Psi_0\rangle$, the bound state and the scattering states $\bar k_2, \ldots, \bar k_{N+1}$ are occupied while the states $\bar k_{N+2}, \ldots, \bar k_{2N}$ are empty. The energy of $|\bar\Psi_0\rangle$ is thus

$$\bar E_0 = \bar\epsilon_b + \bar E_{cb}, \tag{13}$$

where

$$\bar E_{cb} = \sum_{n=2}^{N+1} \bar\epsilon_n \tag{14}$$

is the energy of the half-filled band of scattering states.

From the comparison of E_0 and $\bar E_0$ follows that there is a threshold value ϵ_{d0} given by the condition

$$\epsilon_{d0} + E_{cb} = \bar\epsilon_b + \bar E_{cb}, \tag{15}$$

such that $|\Psi_0\rangle$ is the ground state for $\epsilon_d < \epsilon_{d0}$ while $|\bar\Psi_0\rangle$ is the ground state for $\epsilon_d > \epsilon_{d0}$. It can be shown that $E_{cb} < \bar E_{cb} < E_{cb} + \xi_0$ (see Appendix A). As a consequence, ϵ_{d0} is strictly negative.

The deep state of the above model for x-ray absorption in metals describes an electron which is localized close to the core and which fully screens the core from the conduction electrons. The energy gain of binding such a deep electron should be greater than the gain that results from exposing the delocalized conduction electrons to the core charge. Therefore, the situation of physical interest is given by $\epsilon_d < \epsilon_{d0}$, with $|\Psi_0\rangle$ being the ground state. In Sec. III we will find that it is of technical advantage to study the system at $\tilde\epsilon_d = 0^-$ (with $\tilde\epsilon_d = \epsilon_d + g\xi_0$ denoting the Hartree renormalized deep-state energy) and that the corresponding results can be directly related to those for physically relevant values of ϵ_d.

C. Linear response rate and exciton propagators

In this section, we summarize how the linear response rate of x-ray absorption can be computed from the retarded exciton propagator, and how the retarded, time-ordered and imaginary-time Matsubara exciton propagators are related. This provides the foundation for the Matsubara-formalism-based approach to the absorption rate in subsequent sections.

We suppose that the state of the system at some time t_0 is described by a density operator ϱ (not to be confused with the density of states ρ in the conduction band) that commutes with H and n_d. Later we will focus on the cases $\varrho = |\Psi_0\rangle\langle\Psi_0|$ and $\varrho = e^{-\beta H}/Z$. From t_0 on, the system evolves under the Hamiltonian $H_{tot}(t) = H + H_X(t)$. During that time, $H_X(t)$

induces transitions between the deep state and the conduction band such that the mean deep-state occupancy changes. The linear response rate of this change approaches a long-time limit

$$\frac{d}{dt}\langle n_{\mathrm{d}}\rangle(t) \xrightarrow{t_0 \to -\infty} 2|W|^2 \mathrm{Im}\,\chi^{\mathrm{ret}}(\nu). \tag{16}$$

Here, ν denotes the x-ray frequency and

$$\chi^{\mathrm{ret}}(\nu) = \int_{-\infty}^{\infty} dt\, e^{i\nu t} \chi^{\mathrm{ret}}(t), \tag{17}$$

$$\chi^{\mathrm{ret}}(t) = -i\Theta(t)\langle[A(t)_H, A^\dagger]\rangle \tag{18}$$

denotes the retarded local exciton propagator, with $A(t)_H = e^{iHt}Ae^{-iHt}$. Details on the derivation of this standard result are given in Appendix B.

The above value $2|W|^2 \mathrm{Im}\,\chi^{\mathrm{ret}}(\nu)$ is a good approximation for $d\langle n_{\mathrm{d}}\rangle/dt$ in a certain time regime only: The time span $(t - t_0)$ must be sufficiently long for the linear response rate to approach its long-time limit, and it must be sufficiently short for the linear response approximation to be applicable. The second condition restricts the interval of allowed times by an upper boundary which can be pushed to higher values by decreasing the amplitude W of the perturbation.

Concerning the relation between the retarded and the Matsubara exciton propagator, it will be important later in this section that $\chi^{\mathrm{ret}}(z)$ is analytic in the open upper half of the complex z plane. This region of analyticity of $\chi^{\mathrm{ret}}(z)$ can be established in the usual way by use of the Lehmann representation (see Appendix C). We use z instead of ν to denote complex frequency arguments. The value of $\chi^{\mathrm{ret}}(z)$ at real $z = \nu$ is given by the limit of vanishing imaginary part from above, $\chi^{\mathrm{ret}}(\nu) \equiv \chi^{\mathrm{ret}}(\nu + i\eta)$.

Let use now suppose that the system is initially in the state $\varrho = |\Psi_0\rangle\langle\Psi_0|$. Then one can use $\langle\Psi_0|A^\dagger = 0$ to show that the retarded exciton propagator $\chi_{\Psi_0}^{\mathrm{ret}}(t)$ resulting from that initial state is (for $t \neq 0$) identical to the time-ordered one $\chi_{\Psi_0}(t)$:

$$\chi_{\Psi_0}^{\mathrm{ret}}(t) = -i\Theta(t)\langle\Psi_0|[A(t)_H, A^\dagger]|\Psi_0\rangle \tag{19}$$

$$= -i\Theta(t)\langle\Psi_0|A(t)_H A^\dagger|\Psi_0\rangle \tag{20}$$

$$= -i\langle\Psi_0|\mathcal{T}A(t)_H A^\dagger|\Psi_0\rangle \tag{21}$$

$$=: \chi_{\Psi_0}(t). \tag{22}$$

Here, the time-ordering operator $\mathcal{T}$ rearranges $A(t)_H$ and $A^\dagger = A^\dagger(0)_H$ such that their time arguments decrease from left to right. The time-ordered exciton propagator in frequency representation,

$$\chi_{\Psi_0}(\nu) = \int_{-\infty}^{\infty} dt\, e^{i\nu t} \chi_{\Psi_0}(t), \tag{23}$$

is by definition identical to the particle-hole susceptibility studied in our previous paper [4]; compare also the similar susceptibilities studied in [3,15,16,34,36]. For $\epsilon_{\mathrm{d}} < \epsilon_{\mathrm{d0}}$, the state $|\Psi_0\rangle$ is the ground state. Then

$$-\frac{d}{dt}\langle n_{\mathrm{d}}\rangle(t) \xrightarrow{t_0 \to -\infty} -2|W|^2 \mathrm{Im}\,\chi_{\Psi_0}(\nu) = R(\nu) \tag{24}$$

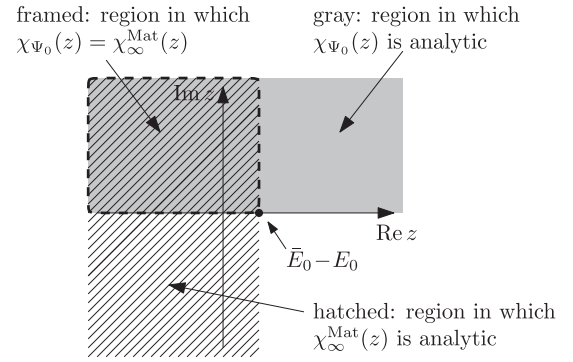is the rate of x-ray induced excitations from the ground state, i.e., the rate of x-ray absorption (compare Ref. [3]).

FIG. 1. Domains of analyticity of $\chi_\infty^{\mathrm{Mat}}(z)$ from Eq. (C9) and $\chi_{\Psi_0}(z) = \chi_{\Psi_0}^{\mathrm{ret}}(z)$ from Eq. (C2) (in the limit $\beta \to \infty$) in the case $\epsilon_{\mathrm{d}} < \epsilon_{\mathrm{d0}}$ in which $|\Psi_0\rangle$ is the ground state.

Next we consider the case that the system is prepared initially in the thermal density operator $\varrho = e^{-\beta H}/Z$ with temperature $T = 1/\beta \neq 0$, chemical potential $\mu = 0$, and with $Z = \mathrm{Tr}\,e^{-\beta H}$. For $\tau \in (-\beta, \beta)$ define the imaginary-time Matsubara exciton propagator

$$\chi_\beta^{\mathrm{Mat}}(\tau) = -\mathrm{Tr}\frac{e^{-\beta H}}{Z}\mathcal{T}A(\tau)_H A^\dagger, \tag{25}$$

with $A(\tau)_H = e^{H\tau}Ae^{-H\tau}$. Here, $\mathcal{T}$ sorts operators with larger imaginary time τ to the left. For bosonic Matsubara frequencies $X_n = 2n\pi/\beta$ define furthermore

$$\chi_\beta^{\mathrm{Mat}}(iX_n) = \int_0^\beta d\tau\, e^{iX_n\tau} \chi_\beta^{\mathrm{Mat}}(\tau). \tag{26}$$

As expected, the Lehmann representation of $\chi_\beta^{\mathrm{Mat}}(iX_n)$ is found to coincide with that of $\chi_\beta^{\mathrm{ret}}(z = iX_n)$ for positive X_n (see Appendix C).

In the limit $\beta \to \infty$ of vanishing temperature, $\chi_\beta^{\mathrm{Mat}}(iX_n)$ approaches a function $\chi_\infty^{\mathrm{Mat}}(iX)$ which is defined on the whole imaginary-frequency axis. The analytic properties of this function are derived in Appendix C. They can be summarized as follows: In the case $\epsilon_{\mathrm{d}} < \epsilon_{\mathrm{d0}}$ in which $|\Psi_0\rangle$ is the ground state, the definition of $\chi_\infty^{\mathrm{Mat}}(z = iX)$ can be extended to the region given by $\mathrm{Re}\,z < \bar{E}_0 - E_0$, which includes the left half plane of z. On the intersection of this domain with the upper half plane, $\chi_\infty^{\mathrm{Mat}}(z)$ coincides with $\chi_{\Psi_0}(z) = \chi_{\Psi_0}^{\mathrm{ret}}(z)$. This makes an analytic continuation from $\chi_\infty^{\mathrm{Mat}}(iX)$ to $\chi_{\Psi_0}(\nu)$ possible. This relation between $\chi_\infty^{\mathrm{Mat}}(z)$ and $\chi_{\Psi_0}(z)$ is sketched in Fig. 1. We remark in passing that in the case $\epsilon_{\mathrm{d}} > \epsilon_{\mathrm{d0}}$ in which $|\bar{\Psi}_0\rangle$ is the ground state, $\chi_\infty^{\mathrm{Mat}}(iX)$ can be analytically continued to the time-ordered exciton propagator $\chi_{\bar{\Psi}_0}(\nu)$ of the system prepared initially in the state $|\bar{\Psi}_0\rangle$.

Later we will find an even simpler relation between $\chi_\infty^{\mathrm{Mat}}$ and χ_{Ψ_0}: For an appropriate choice of ϵ_{d} and in leading-logarithmic approximation holds indeed $\chi_\infty^{\mathrm{Mat}}(iX) = \chi_{\Psi_0}(X)$ (compare Sec. IV B).

III. SPECIFICATIONS OF PERTURBATION THEORY IN MATSUBARA FORMALISM

In this section we specify details of our use of the Matsubara formalism which are crucial for the construction of the

leading-logarithmic one-loop FRG approximation in Sec. IV. While the appearance of fermionic two-particle functions in Sec. III A and the use of Hartree dressed propagators in Sec. III B are completely analogous to our prior treatment in the real-time zero-temperature formalism in Ref. [4], a major difference is that temperature and $\tilde{\epsilon}_{\mathrm{d}}$ now regularize the logarithmic divergencies (Sec. III C). We restrict our considerations to vanishing temperature. In Sec. III D we explain that the particular parquet diagrams involved then allow us to pass over to continuous Matsubara frequencies. Technically we are then so close to the real-time zero-temperature formalism (compare Appendix D) that we can exploit a Ward identity proven in that formalism in Ref. [4] to set $\tilde{\epsilon}_{\mathrm{d}}$ to 0^-; this is explained in Sec. III E.

A. Appearance of fermionic Matsubara Green functions

When we described the relation between χ_{Ψ_0} and $\chi_\beta^{\mathrm{Mat}}$ in the preceding section, we interpreted these susceptibilities as propagators of a single bosonic excitation. Now we aim at a perturbative and, later on, RG approach to the susceptibilities; for that purpose we treat them as fermionic two-particle functions. In fact, it is

$$
\chi_\beta^{\mathrm{Mat}}(iX_n)
$$
$$
= \frac{1}{V} \int_0^\beta d\tau \sum_{kk'} e^{iX_n\tau} G_\beta^{\mathrm{Mat}}(\mathrm{d}, 0; k, \tau | \mathrm{d}, \tau; k', 0) \quad (27)
$$
$$
= \frac{1}{V\beta^3} \sum_{\substack{n_1 n_1' n_2' \\ kk'}} G_\beta^{\mathrm{Mat}}(\mathrm{d}, \omega_{n_1}; k, \omega_{n_1'} + X_n | \mathrm{d}, \omega_{n_1'}; k', \omega_{n_2'}). \quad (28)
$$

Here the fermionic Matsubara two-particle Green function and its representation in terms of Matsubara frequencies are

$$
G_\beta^{\mathrm{Mat}}(l_1, \tau_1; l_2, \tau_2 | l_1', \tau_1'; l_2', \tau_2')
$$
$$
= (-1)^2 \mathrm{Tr}\, \frac{e^{-\beta H}}{Z} \mathcal{T} a_{l_1}(\tau_1)_H a_{l_2}(\tau_2)_H a_{l_2'}^\dagger(\tau_2')_H a_{l_1'}^\dagger(\tau_1')_H, \quad (29)
$$
$$
G_\beta^{\mathrm{Mat}}(l_1, \omega_{n_1}; l_2, \omega_{n_2} | l_1', \omega_{n_1'}; l_2', \omega_{n_2'})
$$
$$
= \int_0^\beta d\tau_1 \cdots \int_0^\beta d\tau_2' \, e^{i(\tau_1\omega_{n_1} + \cdots - \tau_2'\omega_{n_2'})}
$$
$$
\times G_\beta^{\mathrm{Mat}}(l_1, \tau_1; l_2, \tau_2 | l_1', \tau_1'; l_2', \tau_2'). \quad (30)
$$

In these equations, the l_i are single-particle state indices, and time ordering swaps by definition the sign of the expression if the resulting sequence of fermionic ladder operators is an odd permutation of the initial one. In Eq. (30), the $\omega_n = (2n+1)\pi T$ with integer n denote fermionic Matsubara frequencies, and $G_\beta^{\mathrm{Mat}}(l_1, \omega_{n_1}; l_2, \omega_{n_2} | l_1', \omega_{n_1'}; l_2', \omega_{n_2'})$ is proportionate to $\beta\delta_{n_1+n_2, n_1'+n_2'}$.

Standard imaginary-time perturbation theory yields diagrammatic approximations for the fermionic Green functions. The values of the corresponding Hugenholtz diagrams can be determined with the usual Matsubara diagram rules as

$$
\frac{(-1)^P (-1)^{n_{\mathrm{loop}}}}{2^{n_{\mathrm{eq}}} S} \left[\prod (-\bar{v})\right] \left[\prod g_\beta^{\mathrm{Mat}}\right] \quad (31)
$$

(compare, e.g., Ref. [37]). Here, the vertex $\bar{v}_{1'2'|12}$, with indices $1 = (l_1, \tau_1)$, etc., satisfies

$$
\bar{v}_{\mathrm{d}\tau_1', k'\tau_2' | \mathrm{d}\tau_1, k\tau_2} = \frac{U}{V} \delta(\tau_1' - \tau_2') \delta(\tau_2' - \tau_1) \delta(\tau_1 - \tau_2). \quad (32)
$$

Several further components of the vertex are determined through the antisymmetry relation $\bar{v}_{1'2'|12} = \bar{v}_{2'1'|21} = -\bar{v}_{2'1'|12} = -\bar{v}_{1'2'|21}$. All other components of the vertex vanish. In the diagram rule (31), the products run over all vertices and all lines; the latter represent free propagators g_β^{Mat}. Implicitly, all internal indices for states and times or frequencies are to be summed over. $(-1)^P$ is defined as $(+1)$ if the first incoming line of the diagram is connected to the first outgoing line and as (-1) if it is connected to the second outgoing line. n_{loop} is the number of internal closed loops, n_{eq} is the number of pairs of equivalent lines, and S is the diagram symmetry factor.

B. Hartree dressed propagators

The free propagator in Matsubara formalism at finite temperature is given in time or frequency representation, respectively, by

$$
g_\beta^{\mathrm{Mat}}(\tau) = e^{-h\tau}[f(h) - \Theta(\tau - \eta)], \quad (33)
$$
$$
g_\beta^{\mathrm{Mat}}(i\omega_n) = \frac{e^{i\omega_n\eta}}{i\omega_n - h}. \quad (34)
$$

These are equations for matrices. The matrix indices, not written here, refer to single-particle states. In particular, h is the matrix of single-particle energies. Furthermore, $f(h) = (e^{\beta h} + 1)^{-1}$ denotes the (matrix) Fermi function at vanishing chemical potential; Θ denotes the Heaviside step function and η is a positive infinitesimal.

The matrix h does not only comprise the energies ϵ_{d} and ϵ_k appearing in the Hamiltonian in Eq. (6) but also a single-particle perturbation that appears when the interaction term in Eq. (5) is brought into the standard form by permuting all creation operators to the left. At $T = 0$, that perturbation is precisely canceled by the Hartree self-energy. This suggests to work with Hartree dressed propagators, as we already did in our previous analysis of the model within the zero-temperature formalism [4]. Hartree dressed propagators result when h is replaced in Eqs. (33) and (34) by h^{H} with components

$$
h_{k'k}^{\mathrm{H}} = \delta_{k'k}\epsilon_k - [1 - f(\epsilon_{\mathrm{d}})]\frac{U}{V}, \quad (35)
$$
$$
h_{\mathrm{dd}}^{\mathrm{H}} = \epsilon_{\mathrm{d}} + g\xi_0, \quad (36)
$$
$$
h_{\mathrm{d}k}^{\mathrm{H}} = 0 = h_{k\mathrm{d}}^{\mathrm{H}}. \quad (37)
$$

The contribution $-U/V$ to $h_{k'k}^{\mathrm{H}}$ represents the aforementioned single-particle perturbation, while $f(\epsilon_{\mathrm{d}})U/V$ is the Hartree self-energy. In the limit $T \to 0$, these two contributions cancel out due to $f(\epsilon_{\mathrm{d}}) \to 1$. For moderate $T \ll \xi_0$ and for typical $\epsilon_{\mathrm{d}} < -\xi_0$ holds still $1 - f(\epsilon_{\mathrm{d}}) \lll 1$ and the eigenenergies $\tilde{\epsilon}_n$ of $h_{k'k}^{\mathrm{H}}$ can be reasonably approximated by first-order perturbation theory as $\tilde{\epsilon}_n = \epsilon_n - [1 - f(\epsilon_{\mathrm{d}})]U/V$. The first-order shift

$$
[1 - f(\epsilon_{\mathrm{d}})]U/V = [1 - f(\epsilon_{\mathrm{d}})]g\xi_0/N \lll \xi_0/N \quad (38)
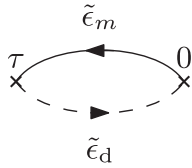$$

FIG. 2. Zeroth-order diagram for $\chi_\beta^{\mathrm{Mat}}(\tau)$. The dashed line denotes a deep-state propagator and the solid line denotes a conduction-state propagator. An extra particle with energy $\tilde{\epsilon}_m$ in the conduction band and a hole at the deep-state energy $\tilde{\epsilon}_d$ propagate from 0 to τ.

is so small that these energies can still be described by a band with density ρ from $-\xi_0$ to ξ_0.

The Hartree self-energy contribution to the deep-state energy in Eq. (36) follows from

$$\frac{U}{V}\rho \int_{-\xi_0}^{\xi_0} d\epsilon\, f(\epsilon) = g\xi_0. \qquad (39)$$

This value is independent of temperature due to $f(\epsilon) + f(-\epsilon) = 1$ and due to the symmetry of the band around the chemical potential $\mu = 0$. We define $\tilde{\epsilon}_d := \epsilon_d + g\xi_0$. The physically relevant case is $\tilde{\epsilon}_d < 0$.

In the following computation of two-particle quantities we will consider only skeleton diagrams with Hartree dressed propagators, without any further self-energy type contributions on the diagram lines. This means that the Hartree dressed propagators take the role of the full single-particle Green functions. Therefore, we will denote the Hartree dressed propagator simply by $G_\beta^{\mathrm{Mat}}(\tau)$ or $G_\beta^{\mathrm{Mat}}(i\omega_n)$, slightly abusing the usual notation for full propagators.

C. Regularizing effect of temperature and $\tilde{\epsilon}_d$

Within the real-time zero-temperature formalism, the archetype of a logarithmic divergence arises in the zeroth-order diagram (with Hartree dressed propagators) to the particle-hole susceptibility. That motivates us to study now the same diagram within Matsubara formalism. We find again a logarithmic divergence; it is, however, regularized by temperature and by $\tilde{\epsilon}_d$.

The zeroth-order contribution to $\chi_\beta^{\mathrm{Mat}}(iX_n)$ at finite temperature and $\epsilon_d < \epsilon_{d0}$ stems from the diagram shown in Fig. 2. It has the value

$$\chi_{0,\beta}^{\mathrm{Mat}}(iX_n) = \int_0^\beta d\tau\, e^{iX_n\tau} \frac{1}{V} \sum_m e^{(\tilde{\epsilon}_d-\tilde{\epsilon}_m)\tau} f(\tilde{\epsilon}_d)[f(\tilde{\epsilon}_m) - 1]$$

$$\qquad (40)$$

$$= \frac{\rho}{V} \int_{-\xi_0}^{\xi_0} d\tilde{\epsilon}\, \frac{f(\tilde{\epsilon}) - f(\tilde{\epsilon}_d)}{\tilde{\epsilon} - \tilde{\epsilon}_d - iX_n}. \qquad (41)$$

To arrive at the second expression we solved the integral over τ and exploited

$$f(\tilde{\epsilon}_d)[f(\tilde{\epsilon}_m) - 1][e^{(\tilde{\epsilon}_d-\tilde{\epsilon}_m)\beta} - 1] = f(\tilde{\epsilon}_d) - f(\tilde{\epsilon}_m). \qquad (42)$$

Furthermore, we used that the Hartree dressed energies $\tilde{\epsilon}_m$ form a band from $-\xi_0$ to ξ_0 with density ρ, as explained above in Sec. III B. In the limit $T \to 0$ holds $f(\tilde{\epsilon}) - f(\tilde{\epsilon}_d) \to$

$-\Theta(\tilde{\epsilon})$ such that

$$\chi_{0,\beta}^{\mathrm{Mat}}(iX_n) \xrightarrow{\beta\to\infty} \chi_{0,\infty}^{\mathrm{Mat}}(iX) = \frac{\rho}{V} \mathrm{Ln}\left(\frac{-\tilde{\epsilon}_d - iX}{\xi_0 - \tilde{\epsilon}_d - iX} \right). \quad (43)$$

Here, Ln denotes the complex logarithm with the branch cut chosen along the negative real axis.

We observe that the logarithmic divergence for $X \to 0$ is regularized by the addend $-\tilde{\epsilon}_d > 0$. An additional regularization appears in the case of finite temperature, where the step of the numerator $f(\tilde{\epsilon}) - f(\tilde{\epsilon}_d)$ in the integrand in Eq. (41) is broadened on a scale of a few T.

In order to keep our analysis simple and comparable to our previous approach within the real-time zero-temperature formalism [4], we focus on the limit of vanishing temperature. In Sec. III D below we describe that this limit can be achieved by the transition from frequency summations to frequency integrations. By this transition we do not only avoid the complication of an additional regularizing scale in form of temperature but also the complication that an RG flow based on a sharp frequency cutoff would perform leaps at the discrete finite-temperature Matsubara frequencies.

There remains to cope with the regularizing effect of $\tilde{\epsilon}_d$. Only after an analytic continuation $iX \mapsto \nu + i\eta = -\tilde{\epsilon}_d + \Delta\nu + i\eta$ with $\Delta\nu \ll \xi_0$ emerges a bare logarithmic divergence in $\Delta\nu/\xi_0$. For higher-order diagrams, too, the logarithmic divergencies appear only after analytic continuation to real frequencies ν close to $-\tilde{\epsilon}_d$. If, however, the internal frequency integrations of a diagram are restricted due to an FRG frequency cutoff, the expressions for the values of higher-order diagrams become more complicated and the analytic continuation becomes more challenging. Then it is difficult to assess whether certain RG approximations capture the leading logarithms. This is considerably more transparent in the case $\tilde{\epsilon}_d = 0^-$, in which the logarithmic divergence of $\chi_{0,\infty}^{\mathrm{Mat}}(iX)$ appears already on the imaginary-frequency axis for $iX \to 0$. Then one can see whether certain RG approximations capture the leading logarithms without analytic continuation to the real-frequency axis. Results for the case $\tilde{\epsilon}_d = 0^-$ are, however, only significant if they can be related to the physically relevant case of finite $\tilde{\epsilon}_d < 0$. In Sec. III E we explain that indeed a direct connection between the two cases is given for the parquet diagrams containing the leading-logarithmic contributions.

D. Zero-temperature limit for parquet diagrams

Within the framework of the real-time zero-temperature formalism it is well known that the leading-logarithmic contributions to the particle-hole susceptibility are given by the parquet diagrams with Hartree dressed lines, in which each bubble comprises one deep-state and one conduction-state propagator [3]. Let us now consider the zero-temperature limit of the same parquet diagrams within Matsubara formalism. In general, the correct zero-temperature limit of any Matsubara diagram is obtained by evaluating the diagram at finite temperature and taking the limit $\beta \to \infty$ of the result. However, the parquet diagrams under consideration are special in being skeleton diagrams with Hartree dressed lines. On the lines connecting the parquet vertices there are no insertions of subdiagrams that represent parts of the self-energy. Due to the

absence of such self-energy type insertions on the propagator lines, the diagram value in the limit $\beta \to \infty$ can be obtained by a different evaluation procedure: In time representation we may evaluate the diagram directly by using the $\beta \to \infty$ limit of the Hartree dressed propagator, namely,

$$G_\infty^{\mathrm{Mat}}(\tau) = e^{-\tilde{\epsilon}\tau}[\Theta(-\tilde{\epsilon}) - \Theta(\tau)], \tag{44}$$

and by integrating imaginary times over the whole axis. Here, the matrix $\tilde{\epsilon}$ is given by $\tilde{\epsilon}_{k'k} = \delta_{k'k}\epsilon_k$ and $\tilde{\epsilon}_{dd} = \epsilon_d + g\xi_0 = \tilde{\epsilon}_d$ and $\tilde{\epsilon}_{dk} = 0 = \tilde{\epsilon}_{kd}$ (compare Sec. III B). In frequency representation we may use the limit propagator

$$G_\infty^{\mathrm{Mat}}(i\omega) = \frac{1}{i\omega - \tilde{\epsilon}} \tag{45}$$

and integrate over continuous Matsubara frequencies instead of summing over discrete ones. For general diagrams, this procedure would miss so-called "anomalous contributions" which take care of interaction-induced changes in the occupancies of the levels [38,39]. Basically, the approach with limit propagators then fails since a series expansion of $\Theta(-\tilde{\epsilon})$ in Eq. (44) around some $\tilde{\epsilon} < 0$ does not provide a valid approximation of $\Theta(-\tilde{\epsilon}_{\mathrm{ren}})$ at some renormalized $\tilde{\epsilon}_{\mathrm{ren}} > 0$. But anomalous contributions arise only in diagrams with self-energy type insertions on the propagator lines, which we do not consider here.

Given a diagram D for the particle-hole susceptibility we now can distinguish the following different ways to evaluate it: as $D_\beta^{\mathrm{Mat}}(iX_n)$ in Matsubara formalism at finite temperature $T = 1/\beta$; as $D_\infty^{\mathrm{Mat}}(iX)$ resulting from $D_\beta^{\mathrm{Mat}}(iX_n)$ in the limit $\beta \to \infty$; as $D_{\mathrm{lp}}^{\mathrm{Mat}}(iX)$ evaluated with the limit propagators from Eq. (44) or (45); and finally as $D_{\Psi_0}(\nu)$ evaluated by use of the real-time zero-temperature formalism as contribution to the particle-hole susceptibility in the state $|\Psi_0\rangle$.

Consider now any single Matsubara diagram $D_{\mathrm{lp}}^{\mathrm{Mat}}(iX)$ for the particle-hole susceptibility that is evaluated with Hartree dressed limit propagators just as described above. For $\tilde{\epsilon}_d < 0$, its value is indeed just the analytic continuation of the value of the very same diagram evaluated as $D_{\Psi_0}(\nu)$ within the real-time zero-temperature formalism; we demonstrate this in Appendix D. Since this way of evaluating Matsubara diagrams at zero temperature is correct for parquet diagrams with Hartree dressed lines and since these diagrams are known to contain all leading-logarithmic contributions to the particle-hole susceptibility in the real-time zero-temperature formalism, we infer that they contain all these contributions also in the Matsubara formalism. The leading-logarithmic contribution to $\chi_\infty^{\mathrm{Mat}}(iX)$ can thus be determined by evaluating parquet diagrams $D_{\mathrm{lp}}^{\mathrm{Mat}}(iX)$ with limit propagators.

E. Setting $\tilde{\epsilon}_d = 0^-$

In Sec. III C we explained that it is technically preferable for the analysis of the leading-logarithmic contributions to work at zero temperature and vanishing $\tilde{\epsilon}_d$. Concerning the temperature, we performed the step to $T = 0$ in Sec. III D where we found that we can use the limit propagators from Eqs. (44) and (45) to evaluate the leading-logarithmic parquet diagrams. Now we focus on $\tilde{\epsilon}_d$ and argue that the diagram values resulting for the technically desirable choice

$\tilde{\epsilon}_d = 0^-$ are directly related to the physically relevant case of finite $\tilde{\epsilon}_d < 0$.

In Appendix D we show that diagrams $D_{\mathrm{lp}}^{\mathrm{Mat}}(z)$ for the particle-hole susceptibility $\chi_\infty^{\mathrm{Mat}}(z)$ evaluated within the Matsubara formalism using limit propagators are, in the region $\mathrm{Im}\,z > 0$ and $\mathrm{Re}\,z < -\tilde{\epsilon}_d$, identical to the same diagrams evaluated within the real-time zero-temperature formalism. In the special case $\tilde{\epsilon}_d = 0^-$ this region still includes the upper half of the imaginary z axis. Furthermore, in Ref. [4] we described that a Ward identity connects the results for $\chi_{\Psi_0}(\nu)$ computed within the real-time zero-temperature formalism for $\tilde{\epsilon}_d < 0$ and for $\tilde{\epsilon}_d = 0$ in the form $\chi_{\Psi_0}(\nu, \tilde{\epsilon}_d) = \chi_{\Psi_0}(\nu + \tilde{\epsilon}_d, 0)$ (see also [3]). This identity holds diagram by diagram. It follows for any parquet diagram $D(\nu, \tilde{\epsilon}_d)$ for the susceptibility with Hartree dressed lines and real-valued $X > 0$ and ν that

$$D_{\mathrm{lp}}^{\mathrm{Mat}}(iX, 0^-)|_{iX \to \nu + i\eta} = D_{\Psi_0}(\nu, 0) = D_{\Psi_0}(\nu - \tilde{\epsilon}_d, \tilde{\epsilon}_d). \tag{46}$$

Here, the analytic continuation induced by $iX \to \nu + i\eta$ requires formally $\nu < 0$. However, we can directly extend the result to $\nu > 0$ because $D_{\Psi_0}(\nu, 0)$ allows for an analytic continuation from $\nu < 0$ to $\nu > 0$ via the upper half plane. The same result then holds for the leading-logarithmic parquet approximation to χ as sum over such diagrams. It provides a direct connection between the leading-logarithmic Matsubara susceptibility computed at $\tilde{\epsilon}_d = 0^-$ with limit propagators and the leading-logarithmic ground-state susceptibility at physically relevant values of $\tilde{\epsilon}_d < 0$. Therefore, we can restrict our Matsubara analysis to the case $\tilde{\epsilon}_d = 0^-$, using the deep-state propagator

$$G_{\infty,\mathrm{d}}^{\mathrm{Mat}}(i\omega) = \frac{1}{i\omega - 0^-}. \tag{47}$$

We note that this argument does not rely on whether $\tilde{\epsilon}_d = 0^-$ implies $\epsilon_d < \epsilon_{d0}$ or not.

IV. LEADING-LOGARITHMIC APPROXIMATION BY ONE-LOOP FRG

In this section we construct a one-loop Matsubara FRG approximation to the model at hand which reproduces identically the leading-logarithmic parquet approximation of Ref. [3]. We start with an approximation to the local conduction-electron propagator which we take over from Refs. [15,16,36] and which we show to comply with the leading-logarithmic approximation. The decisive step is then to realize that this approximation makes the computational expressions for the Matsubara diagrams for $\chi_\infty^{\mathrm{Mat}}(iX)$ coincide completely with those for the real-time zero-temperature diagrams for $\chi_{\Psi_0}(X)$. From that point on we can copy identically all approximation steps that we performed in our previous real-time zero-temperature approach from Ref. [4].

A. Approximation to the local conduction-electron propagator

In this subsection we make and justify an approximation for the conduction-electron propagator which was already used in Refs. [15,16,36]; there it was motivated cursorily but not justified in detail. We show that this approximation does not affect the leading logarithms.

Consider some parquet diagram $D_{\text{lp}}^{\text{Mat}}(iX)$ within Matsubara formalism, with lines representing the zero-temperature limit G_∞^{Mat} of the deep-state propagator or the Hartree dressed conduction-electron propagator, respectively. Since the value of a bare vertex is independent of the momenta of the attached conduction-electron lines, all momentum summations appearing in the diagram are independent of each other. Therefore, these summations can be performed separately for each conduction-electron line, leading to the local conduction-electron propagator

$$G_{\infty,\text{c}}^{\text{Mat}}(i\omega) = \frac{1}{V} \sum_k G_{\infty,k}^{\text{Mat}}(i\omega) \tag{48}$$

$$= \frac{\rho}{V} \int_{-\xi_0}^{\xi_0} \frac{d\tilde{\epsilon}}{i\omega - \tilde{\epsilon}} \tag{49}$$

$$= -2i \frac{\rho}{V} \arctan \frac{\xi_0}{\omega} \tag{50}$$

$$= -i\pi \frac{\rho}{V} \left[\text{sgn}(\omega) - \frac{2}{\pi} \arctan \frac{\omega}{\xi_0} \right]. \tag{51}$$

We follow Refs. [15,16,36] in approximating $G_{\infty,\text{c}}^{\text{Mat}}(i\omega)$ as

$$G_{\infty,\text{c}}^{\text{Mat}}(i\omega) \approx -i\pi \frac{\rho}{V} \text{sgn}(\omega) \Theta(\xi_0 - |\omega|). \tag{52}$$

Let us make sure that this approximation does not affect the leading logarithms. For that purpose we consider one of the bubbles in a leading parquet diagram. We assume it to be a particle-hole bubble with one deep-state line and one conduction-electron line; the argument can be applied analogously to the remaining case of a particle-particle bubble. The value of the particle-hole bubble is determined by the integral

$$\int_{-\infty}^{\infty} \frac{d\omega}{2\pi} G_{\infty,\text{d}}^{\text{Mat}}(i\omega) G_{\infty,\text{c}}^{\text{Mat}}[i(\omega + X)] f(\omega). \tag{53}$$

Here, X denotes the bosonic exchange frequency of the bubble. The function $f(\omega)$ results from the more inner bubbles that are contained in the effective vertices at the two ends of our particle-hole bubble. f depends in general on X and on the external frequencies of the bubble; this dependence is not shown in our notation. For $|\omega|/\xi_0 \to \infty$ and for ω approaching certain ω_j which depend on X and on the external frequencies of our bubble, $f(\omega)$ diverges like some power of a logarithm. When combined with the two propagators in Eq. (53), the factor $f(\omega)$ does not lead to a divergence of the integral. In the next two paragraphs we concentrate on the case $|X| \ll \xi_0$ and argue afterwards that this is indeed the relevant case.

Both propagators in the integrand in Eq. (53) fall off as $1/\omega$ for $|\omega|/\xi_0 \to \infty$ so that the contribution from large frequencies $|\omega| \gtrsim \xi_0$ to the integral is $O(1)$. Therefore, we can neglect the contribution from this frequency region. The lower bound for the negligible region of $|\omega|$ is somewhat arbitrary; the only condition is that ω with $|\omega| \ll \xi_0$ are not neglected. In particular the negligible region can be chosen as $|X + \omega| \geqslant \xi_0$ which justifies the step function in Eq. (52). We note that such a cutoff in the approximated propagator is required: An insertion of the propagator from Eq. (52) without the step function into the integral in Eq. (53) would cause the contribution from large frequencies $|\omega| \gtrsim \xi_0$ to diverge.

The leading-logarithmic contributions to the integral in Eq. (53) originate from the combination of the factor $G_{\infty,\text{d}}^{\text{Mat}}(i\omega) = 1/(i\omega - 0^-)$ with the discontinuous function $\text{sgn}(\omega + X)$ contained in $G_{\infty,\text{c}}^{\text{Mat}}[i(\omega + X)]$ in Eq. (51). In fact, this mechanism of how the logarithmic divergencies arise is the same as in the zero-temperature formalism (cf. Sec. III D of Ref. [4]). The important frequency range is given by $|X| \leqslant |\omega| \ll \xi_0$, where we can approximate

$$G_{\infty,\text{c}}^{\text{Mat}}[i(\omega + X)] \approx -i\pi \frac{\rho}{V} \text{sgn}(\omega + X). \tag{54}$$

A straight computation shows that the next correction term to $G_{\infty,\text{c}}^{\text{Mat}}[i(\omega + X)]$, which is of order $(X + \omega)/\xi_0$, yields only a subleading contribution.

We still need to justify that we restricted our considerations to the case $|X| \ll \xi_0$. The argument will first be given for the outermost bubbles in a diagram for the particle-hole susceptibility. Then it can be replicated iteratively for the more and more inner tiers. To start with, the leading-logarithmic approximation for the susceptibility $\chi_\infty^{\text{Mat}}(iX)$ is good only for $|X| \ll \xi_0$, for which the logarithms become large. This corresponds to the fact that after an analytic continuation $iX \to \nu + i\eta$ we are interested in the behavior of $\chi(\nu)$ near threshold. Now, the bosonic exchange frequency X_1 of the outermost bubbles in a diagram $D_{\text{lp}}^{\text{Mat}}(iX)$ contributing to $\chi_\infty^{\text{Mat}}(iX)$ is equal to X and thus $|X_1| \ll \xi_0$. Concerning the next inner bubbles, we consider some "crossed" particle-particle bubble which may be contained in the effective vertex between two outermost particle-hole bubbles. If we call the integration frequencies of these outermost particle-hole bubbles ω_1 and ω_1', then the crossed particle-particle bubble has the bosonic total frequency $\Omega_2 = \omega_1 + \omega_1' + X_1$. We discussed above that the important range of frequency integration in the particle-hole bubbles is given by $|X_1| \leqslant |\omega_1^{(\prime)}| \ll \xi_0$. Hence, $|\Omega_2| \ll \xi_0$ for the important contributions. In turn, the leading contributions to the value of the particle-particle bubble arise from a frequency integration over ω_2 with $|\Omega_2| \leqslant |\omega_2| \ll \xi_0$; this can be shown on the analogy of the above discussion for the particle-hole bubble. If now the effective vertex between two particle-particle bubbles with integration frequencies ω_2 and ω_2' contains a more inner, crossed particle-hole bubble, then the latter one is characterized by the bosonic exchange frequency $X_3 = \Omega_2 - \omega_2 - \omega_2'$ which again satisfies $|X_3| \ll \xi_0$. This argument can be repeated on and on to show that the leading contributions result only from those internal integration frequencies for which the natural bosonic frequencies X_i, Ω_i of all inner bubbles are much smaller that ξ_0.

B. Identity between leading-logarithmic contributions in real and imaginary time

In this subsection we study the consequences of approximation (52). We find that the approximate expressions that we obtain for the Matsubara diagrams of the particle-hole susceptibility on the imaginary-frequency axis are plainly identical (without analytic continuation) to the ones known from the real-time zero-temperature approach on the real axis. This makes it possible to use just the identical FRG approximation steps as used in the real-time case in Ref. [4].

First we observe that the approximated local conduction-electron propagator from Eq. (52) coincides with the imaginary part of the local conduction-electron propagator $G_c(\omega)$ from the real-time zero-temperature formalism,

$$G_c(\omega) = \frac{\rho}{V}\left[\ln\frac{|\xi_0 + \omega|}{|\xi_0 - \omega|} - i\pi\,\mathrm{sgn}(\omega)\Theta(\xi_0 - |\omega|)\right]. \quad (55)$$

The imaginary part of this propagator is indeed the only part that was retained during the leading-logarithmic calculations in the real-time zero-temperature formalism (see Refs. [3,4]).

Furthermore, the deep-state propagator in Eq. (47) is, up to a factor $(-i)$, identical to the deep-state propagator used in the treatment of the model with the real-time zero-temperature formalism (see Refs. [3,4]). We note that the particular choice $\tilde{\epsilon}_d = 0^-$ is responsible for this match between $1/(i\omega - \tilde{\epsilon}_d)$ and $(-i)/(\omega - \tilde{\epsilon}_d - i0^+)$.

The diagram rules for the susceptibility in Matsubara formalism differ from those in the real-time zero-temperature formalism by a global factor i and by factors i for each vertex. All these factors i together precisely compensate the factors $(-i)$ in the deep-state propagators. As a consequence, the resulting expressions for the Matsubara diagrams $D_{lp}^{Mat}(iX)$ computed with approximated local conduction-electron propagators are literally identical to those for the diagrams for $\chi_{\Psi_0}(X)$ in the real-time zero-temperature formalism.

This conformance needs to be distinguished from the analytic continuation between χ_∞^{Mat} and χ_{Ψ_0}: Without the approximation (52) for the Matsubara conduction-electron propagator, the diagrams $D_{lp}^{Mat}(z)$ for $\chi_\infty^{Mat}(z)$ are identical in value to those for $\chi_{\Psi_0}(z)$ in the upper left quadrant of z (see Appendix D). In particular the diagrams $D_{lp}^{Mat}(iX)$ have the same values as the diagrams for $\chi_{\Psi_0}(iX)$, not as those for $\chi_{\Psi_0}(X)$ as found above. However, in the leading-logarithmic approximation the diagram values for $\chi_{\Psi_0}(iX)$ and for $\chi_{\Psi_0}(X)$ can both be reduced to the same factors of the form $\ln|X|/\xi_0$ and are thus identical. This can be understood from the result

$$\chi_{\Psi_0}(z) = \frac{\rho}{2g}\left[1 - \left(-\frac{\xi_0}{z + \tilde{\epsilon}_d}\right)^{2g}\right], \quad (56)$$

which was constructed in Ref. [3] by imposing the desired analytic properties onto the leading-logarithmic approximation. According to this result, the leading contribution to $\chi_{\Psi_0}(X)$ and that to $\chi_{\Psi_0}(iX)$ at $\tilde{\epsilon}_d = 0^-$ read both as $\rho[1 - (\xi_0/|X|)^{2g}]/(2g)$.

For the simple example of the noninteracting particle-hole susceptibility, the peculiar approximate identity between $\chi_\infty^{Mat}(iX)$ and $\chi_{\Psi_0}(X)$ is traced back to the pole structure of the integrand in the complex plane in Appendix E.

C. Adopting the steps from the real-time zero-temperature approach

Given the identity between the approximate expressions for the diagrams $D_{lp}^{Mat}(iX)$ for $\chi_\infty^{Mat}(iX)$ and those for $\chi_{\Psi_0}(X)$, it is straightforward to construct a one-loop Matsubara FRG approximation that captures all leading logarithms: We can copy one by one the steps from the zero-temperature FRG approach of Ref. [4]. Here we summarize these steps only very briefly; for details see Sec. V of Ref. [4].

First, we introduce a sharp frequency cutoff into the principal-value part of the Hartree dressed deep-state propagator:

$$G_{\infty,d}^{Mat,\lambda}(i\omega) = -i\Theta(|\omega| - \lambda)\frac{1}{\omega} + \pi\delta(\omega). \quad (57)$$

Then the conduction-state propagator at the initial flow parameter $\lambda_{ini} \to \infty$ proves to be Hartree dressed. We approximate this propagator by Eq. (52). In leading-logarithmic order the initial value of the (one-particle irreducible) two-particle vertex function is given by the bare interaction while all higher vertex functions vanish.

Next we neglect the flow of the self-energy of the three-particle vertex function and of the two-particle vertex function with four deep-state indices. In the flow equations for the two-particle vertex function with two deep-state and two conduction-state indices we perform the logarithmic approximation by setting, e.g., $|\omega + \lambda - \Omega| \approx \max\{|\omega|, \lambda\}$ in the frequency arguments of the vertex functions. Furthermore, we approximate the start of the flow by setting, e.g., $\Theta(\xi_0 - |\Omega + \lambda|) \approx \Theta(\xi_0 - \lambda)$.

As shown in Ref. [4], we then obtain the identical integral equations for the two-particle vertex function as in Ref. [3]. We copy the steps for its solution and for the computation of the susceptibility and obtain

$$\chi_\infty^{Mat}(iX) = \frac{\rho}{2g}\left[1 - \left(\frac{\xi_0}{|X|}\right)^{2g}\right]. \quad (58)$$

We identify this function with the analytic continuation of the retarded ground-state susceptibility $\chi_\infty^{Mat}(iX) = \chi_{\Psi_0}^{ret}(iX) = \chi_{\Psi_0}(iX)$ (see Sec. II C). Then the only difference compared to Refs. [3,4] is that we obtain the result (58) for $\chi_{\Psi_0}(iX)$ instead of $\chi_{\Psi_0}(X)$. This difference is of no importance: We can reconstruct the imaginary part of $\chi_{\Psi_0}(z)$ in the same way as Ref. [3], namely, such that the branch cut of the function is located on the positive semiaxis, as required. We end up again with Eq. (56).

V. COMPARISON TO REF. [16]

In Ref. [16] the same model of x-ray absorption is investigated with different one-loop and multiloop FRG approximations. Reference [16] presents data which show that, compared to one-loop FRG, multiloop iterations improve the agreement of the FRG results with those of a numerical solution of the parquet approximation. We should now clarify how this relates to our construction of a one-loop Matsubara FRG scheme that reproduces identically the leading-logarithmic parquet approximation of Roulet *et al.* [3]. There are two possible explanations for the improved agreement between multiloop FRG and the numerical parquet results which is observed in Ref. [16]. One is that the one-loop FRG approximations of Ref. [16] are not constructed properly and miss certain leading contributions. The other is that the numerical improvements due to multiloop FRG in Ref. [16] are subleading and thus beyond the controlled regime of the parquet approximation.

The second possibility is actually very plausible. We note that due to several approximations in the analytic evaluation, even the leading-logarithmic parquet result of Roulet *et al.*

differs subleadingly from the numerically evaluated sum of the parquet diagrams. On the subleading level both approximations are uncontrolled and none is thus preferable *a priori*. Figure 4(d) of Ref. [16] displays the particle-hole susceptibility at zero imaginary frequency as function of the interaction strength. According to this figure, the agreement between the leading-logarithmic result of Roulet *et al.* and the numerical sum of the parquet diagrams is fine for interactions up to roughly $g = 0.2$, while larger values of g (called u in that reference) lead to sizable differences. The figure caption attributes the differences to subleading contributions; they are thus in the uncontrolled regime. In this context we note that while the choice $2g - g^2$ for the exponent of the guide-to-the-eye lines in this figure represents the correct function in second order (compare Ref. [35]), it is uncontrolled in the parquet approximation; the correction $-g^2$ was even renounced in the improved self-consistent treatment of Ref. [34]. If we concentrate on $g = 0.28$, we find for $|\chi^{\text{Mat}}(iX=0)|$ from Fig. 4 of Ref. [16] approximately 7ρ for the numerical parquet computation and approximately 9ρ for the leading-logarithmic result of Roulet *et al.* The difference of about 2ρ between these values highlights the large influence of subleading contributions. From the ordinate intercepts in Fig. 5 of Ref. [16] we infer that the one-loop FRG results for $|\chi^{\text{Mat}}(iX=0)|$ depend on the choice of regulator and are roughly in the range from 8.5ρ to 11ρ. This differs again up to 2ρ from the 9ρ corresponding to the solution of Roulet *et al.* It is hence reasonable to assume that all approximations with different loop orders studied in Ref. [16] differ only subleadingly.

In spite of this finding we have the impression that the regulators chosen in Ref. [16] are not optimal for a one-loop FRG. They suffer from the drawback that the dependence of the regulator dressed deep-state propagators on ω and ϵ_{d} is not restricted to a function of $i\omega - \epsilon_{\text{d}}$ alone. In fact, the regulator-free bare deep-state propagator $1/(i\omega - \epsilon_{\text{d}})$ is a function of $i\omega - \epsilon_{\text{d}}$ only. This property ensures that the particle-hole susceptiblity $\chi^{\text{Mat}}(z)$ is a function of $z + \epsilon_{\text{d}}$ (compare Sec. III C of Ref. [4]). This Ward identity related to particle-number conservation and time translational invariance is satisfied not only by the exact result, but also by any single diagram, by the sum of the parquet diagrams and by the leading-logarithmic result from Eq. (56). Correspondingly, the very logarithmic divergencies appearing in perturbation theory are of the form $\ln[(z + \epsilon_{\text{d}})/\xi_0]$ and are thus divergencies in $z + \epsilon_{\text{d}}$. The different regulators investigated in Ref. [16] destroy this property. Among those is, for example, a sharp frequency cutoff in the deep-state propagator,

$$G_{\text{d}}^{\lambda}(i\omega_n) = \Theta(|\omega_n| - \lambda)\frac{1}{i\omega_n - \epsilon_{\text{d}}}, \tag{59}$$

with λ denoting the flow parameter. Here, the cutoff prefactor $\Theta(|\omega_n| - \lambda)$ is not a function of $(i\omega_n - \epsilon_{\text{d}})$. The resulting defect of the one-loop approximation is healed by the multiloop iterations since they make the particle-hole susceptibility converge to the sum of the parquet diagrams. The Ward identity is then satisfied again so that the nature of the divergencies can be captured.

We note in passing that our one-loop flow induced by the cutoff from Eq. (57) is not affected by this problem. As we set $\tilde{\epsilon}_{\text{d}} = 0^-$, the result of the flow depends on z alone. After

the flow, the use of Eq. (46) allows for the transition from z to $z + \tilde{\epsilon}_{\text{d}}$, which then appears correctly in Eq. (56).

In summary, Ref. [16] demonstrates with specific examples that the multiloop FRG scheme allows to construct the sum of the parquet diagrams even by use of cutoffs whose suitability for the model was not inspected in detail. The resulting numerical parquet approximation is then automatically guaranteed to contain the leading-logarithmic contributions. In the present paper we demonstrated how the leading-logarithmic parquet approximation can also be obtained from a well-constructed one-loop FRG flow. This shows that no general superiority of multiloop flows over one-loop flows is given for the model at hand.

VI. CONCLUSION

The leading-logarithmic parquet approximation for certain zero- and one-dimensional condensed-matter problems is a prominent example of a controlled approximation in a regime not accessible by perturbation theory. In a previous paper [4] we revealed that a suitably constructed, one-loop truncated fermionic FRG approximation merges with the leading-logarithmic parquet approximation of Roulet *et al.* for x-ray absorption in metals [3]. This highlights the capability of the fermionic FRG to generate controlled nonperturbative approximations, in contrast to the perturbatively or *a posteriori* justified truncations which are currently widely used [9,13] in fermionic condensed-matter FRG studies. The potential of the fermionic FRG to provide controlled approximations should now be systematically developed. The first important step is to transfer the construction of a leading-logarithmic one-loop FRG from the zero-temperature formalism used in Ref. [4] to the Matsubara formalism, which is most broadly used for applications of the FRG to condensed-matter problems [9–13]. This is what we achieved in this paper.

We demonstrated how to construct a one-loop FRG approximation within Matsubara formalism that leads to the known leading-logarithmic approximation for the absorption of x rays in metals. Our approach is founded on the fact that the leading approximation for the particle-hole susceptibility $\chi_{\Psi_0}(z)$ is identical on the real and on the imaginary z axis when $\tilde{\epsilon}_{\text{d}}$ is set to zero [see Eq. (58)]. Due to this property it was possible to find an approximate formulation of the Matsubara perturbation theory at $T = 0$ which leads to imaginary-frequency expressions that are identical to the real-frequency expressions from the zero-temperature ground-state formalism. At that stage we could copy all further steps from Ref. [4].

We thus substantiated that, also within Matsubara formalism, leading-logarithmic approximations can be achieved by one-loop FRG approximations. We expect that a generalization of our one-loop flow to $T > 0$ is possible in a natural way by using discrete Matsubara frequencies and then, potentially, resorting to a numerical solution. This would allow to study how the temperature-induced regularization of the divergencies influences observables. For $T \to 0$ the results of such an approach are expected to converge to those of the continuous-frequency approach presented in this paper. Furthermore, we expect that our analysis can be transferred to models whose structure of logarithmic divergencies in per-

turbation theory resembles that of the x-ray absorption model, in particular to the Kondo model and to the Fermi gas model of one-dimensional conductors.

We pointed out that the multiloop corrections to the one-loop results in Ref. [16] are of a size corresponding to subleading contributions. This is, however, not important for the main message of that reference, which is that the multiloop scheme ensures the numerical summation of the complete parquet diagrams for any choice of cutoff. The approximation resulting from that summation is known to satisfy certain symmetries, sum rules, and conservation laws [40–42]. This was beneficial for multiloop FRG studies of two-dimensional systems of correlated electrons [43–45] and three-dimensional interacting quantum spin systems [46,47]. But concerning the particular class of systems represented by the x-ray absorption model with its plain structure of logarithmic divergencies, we established that the desirable leading-logarithmic approximation can be achieved even analytically by a suitably constructed one-loop FRG.

A broad field of future investigations opens up on the basis of our present study. From a methodological point of view, two extensions are highly desirable: on the one hand, that to a consistent handling of subleading contributions, on the other hand, that to the nonequilibrium Keldysh formalism. From an applications point of view, our scheme awaits to be adapted to the study of diverse zero- and one-dimensional quantum-dot systems at low temperatures in and out of equilibrium. A long-term goal is the construction of an efficient and analytically transparent impurity solver whose range of applicability extends from the perturbative to the Kondo regime.

APPENDIX A: DETAILS ON THE STATE $|\bar{\Psi}_0\rangle$

In Sec. II B we described that the ground state of the system filled with $(N + 1)$ particles is either the state $|\Psi_0\rangle$ in which the deep level and the N states in the lower half of the conduction band of momentum states are occupied, or the state $|\bar{\Psi}_0\rangle$ in which a bound state and N states in the lower part of the band of scattering states are occupied. The bound state and the scattering states are single-particle eigenstates of the perturbed Hamiltonian

$$\bar{H}_0 = \sum_{k,k'} \left(\delta_{kk'} \epsilon_k - \frac{U}{V} \right) a_{k'}^\dagger a_k. \tag{A1}$$

Here we analyze these eigenstates of $\bar{H}_0$ in more detail.

The single-particle energies of $\bar{H}_0$ are the eigenvalues $\bar{\epsilon}_n$ of the matrix with components $\bar{\epsilon}_{kk'} = \delta_{kk'} \epsilon_k - U/V$. First-order perturbation theory yields

$$\bar{\epsilon}_n = \epsilon_n - \frac{g}{\rho} + O(g^2), \quad n = 1, \dots, 2N \tag{A2}$$

with $\epsilon_n \equiv \epsilon_{k_n}$ denoting the unperturbed energies and with $g = \rho U/V$. In order to analyze $\bar{\epsilon}_n$ beyond perturbation theory we introduce a discrete model for the band of unperturbed mo-
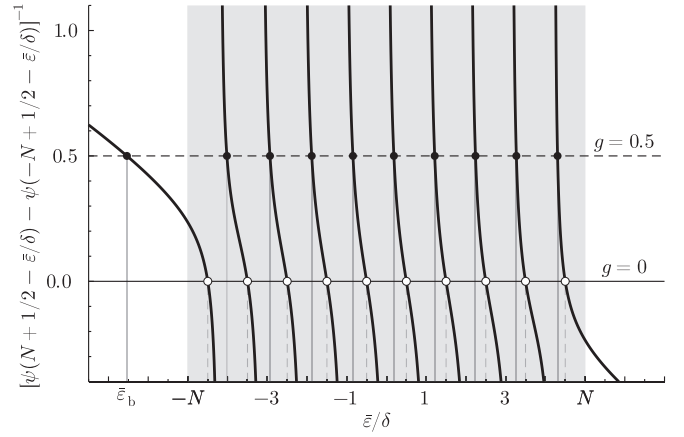

FIG. 3. Graphical solution of the implicit equation (A4) for the case $N = 5$. (The value $N = 5$ is sufficiently small to make the details visible and sufficiently large to convey the impression of a band of states. Realistic values of N would be much larger.) The empty circles mark singularities of the denominator $\psi(N + \frac{1}{2} - \bar{\epsilon}_n/\delta) - \psi(-N + \frac{1}{2} - \bar{\epsilon}_n/\delta)$, corresponding to the positions of the unperturbed energies $\epsilon_n = (n - N - \frac{1}{2})\delta$ at $g = 0$. The gray region visualizes the corresponding energy window of the unperturbed conduction band. The black dots show the solutions of the implicit equation for $g = 0.5$ and thus mark the positions of the corresponding perturbed energies $\bar{\epsilon}_n$.

mentum states: We set $\epsilon_n = (n - N - \frac{1}{2})\delta$, $n = 1, \dots, 2N$, with a constant level spacing $\delta > 0$. If δ is much smaller than all other energies of interest, this discrete band can be treated as a continuous conduction band with half-width $\xi_0 = N\delta$ and density of states $\rho = 1/\delta$. For the discrete model, a straightforward computation of the roots $\bar{\epsilon}_n$ of the characteristic polynomial of $\bar{H}_0$ in the single-particle sector leads to the implicit equation

$$g = \left(\sum_{j=0}^{2N-1} \frac{1}{j - N + \frac{1}{2} - \bar{\epsilon}_n/\delta} \right)^{-1} \tag{A3}$$

$$= \left[\psi\left(N + \frac{1}{2} - \bar{\epsilon}_n/\delta\right) - \psi\left(-N + \frac{1}{2} - \bar{\epsilon}_n/\delta\right) \right]^{-1}, \tag{A4}$$

with $g = U/(V\delta) \neq 0$, and with the digamma function ψ used in the second line to express the sum appearing in the first line; for details on the digamma function see Chap. 5 of Ref. [48]. This implicit equation has $2N$ solutions $\bar{\epsilon}_n$, $n = 1, \dots, 2N$. A graphical solution makes evident that

$$\bar{\epsilon}_1 < \epsilon_1 \quad \text{and} \quad \epsilon_{n-1} < \bar{\epsilon}_n < \epsilon_n, \quad n = 2, \dots, 2N \tag{A5}$$

(see Fig. 3).

Of particular interest is the energy $\bar{\epsilon}_b := \bar{\epsilon}_1$ of a bound state that results from the localized attractive potential generated by the deep hole. An approximation for $\bar{\epsilon}_b$ that applies to those values of g which are relevant for our paper can be derived from $\psi(x) \approx \ln x$ for $x \gg 1$. Under the assumption $-N + \frac{1}{2} - \bar{\epsilon}_b/\delta \gg 1$ this approximation can be applied to Eq. (A4), yielding

$$\frac{1}{g} \approx \ln \frac{N + \frac{1}{2} - \bar{\epsilon}_b/\delta}{-N + \frac{1}{2} - \bar{\epsilon}_b/\delta} \tag{A6}$$

with the solution

$$\bar{\epsilon}_b \approx \left(-N + \frac{1}{2}\right)\delta - \frac{2N\delta}{e^{1/g} - 1} \approx -\xi_0(1 + 2e^{-1/g}). \quad (A7)$$

The last approximation step in Eq. (A7) requires additionally $g \ll 1$. In total, the above approximation for $\bar{\epsilon}_b$ is good for $1 \gg g \gg 1/\ln(2N) = 1/\ln(2\xi_0\rho)$.

In the $(N + 1)$-particle state $|\bar{\Psi}_0\rangle$, the bound state and the states $\bar{k}_2, \ldots, \bar{k}_{N+1}$ are occupied, while the states $\bar{k}_{N+2}, \ldots, \bar{k}_{2N}$ are empty. The energy of $|\bar{\Psi}_0\rangle$ is thus

$$\bar{E}_0 = \bar{\epsilon}_b + \bar{E}_{cb}, \quad (A8)$$

where

$$\bar{E}_{cb} = \sum_{n=2}^{N+1} \bar{\epsilon}_n \quad (A9)$$

is the energy of the half-filled band of scattering states. From the inequality (A5) follows

$$E_{cb} < \bar{E}_{cb} < E_{cb} + \xi_0. \quad (A10)$$

The difference in energy of the half-filled band of scattering states and the half-filled band of plane-wave states, $\bar{E}_{cb} - E_{cb}$, is thus less than the single-particle energy ξ_0.

APPENDIX B: LINEAR RESPONSE RATE

In Sec. II C we reported that the mean occupancy of the deep level changes under the influence of the x-ray field as

$$\frac{d}{dt}\langle n_d \rangle(t) \xrightarrow{t_0 \to -\infty} 2|W|^2 \text{Im}\chi^{\text{ret}}(\nu) \quad (B1)$$

in linear response. Here we give some details on the derivation.

The rate of change of the mean deep-state occupancy is

$$\frac{d}{dt}\langle n_d \rangle(t) = \frac{d}{dt}\langle U_{\text{tot}}(t_0, t)n_d U_{\text{tot}}(t, t_0)\rangle \quad (B2)$$

$$= i\langle U_{\text{tot}}(t_0, t)[H_X(t), n_d]U_{\text{tot}}(t, t_0)\rangle \quad (B3)$$

$$= i\langle U_I(t_0, t)[H_X, n_d](t)_H U_I(t, t_0)\rangle. \quad (B4)$$

Here, $\langle\cdot\rangle = \text{Tr}(\varrho\cdot)$ denotes the expectation value given the density operator ϱ. Furthermore, U_{tot} denotes the time-evolution operator under the total Hamiltonian $H_{\text{tot}}(t) = H + H_X(t)$, and $U_I(t', t) = U_H(0, t')U_{\text{tot}}(t', t)U_H(t, 0)$ denotes the interaction-picture time-evolution operator, with U_H referring to time evolution under H only. Furthermore,

$$[H_X, n_d](t)_H = U_H(0, t)[H_X(t), n_d]U_H(t, 0) \quad (B5)$$

is the commutator in the interaction picture. By use of the lowest-order approximation

$$U_I(t, t_0) = 1 - i \int_{t_0}^t dt_1 H_X(t_1)_H \quad (B6)$$

we obtain

$$\frac{d}{dt}\langle n_d \rangle(t) = i\langle[H_X, n_d](t)_H\rangle$$

$$+ \int_{t_0}^t dt_1 \langle[[H_X, n_d](t)_H, H_X(t_1)_H]\rangle. \quad (B7)$$

The first addend on the right-hand side vanishes since the density operator is supposed to commute with H and n_d. For the second addend we employ

$$\langle[[H_X, n_d](t)_H, H_X(t_1)_H]\rangle = -2|W|^2 \text{Re}e^{i\nu(t-t_1)}$$
$$\times \langle[A(t-t_1)_H, A^\dagger]\rangle \quad (B8)$$

to obtain

$$\frac{d}{dt}\langle n_d \rangle(t) = -2|W|^2 \text{Re} \int_0^{t-t_0} dt' \, e^{i\nu t'}\langle[A(t')_H, A^\dagger]\rangle \quad (B9)$$

$$\xrightarrow{t_0 \to -\infty} 2|W|^2 \text{Im}\chi^{\text{ret}}(\nu), \quad (B10)$$

as indicated in Sec. II C.

APPENDIX C: ANALYTIC BEHAVIOR OF EXCITON PROPAGATORS

In Sec. II C we reported in which regions the retarded and Matsubara exciton propagator are analytic and where they coincide. In this part of the Appendix we derive these statements from the Lehmann representation of the propagators.

By use of the Lehmann representation it is straightforward to show that $\chi^{\text{ret}}(z)$ is analytic in the open upper half plane of z. For that purpose, let $|m\rangle$ denote the states of an orthonormal basis of common eigenstates of H and ϱ, with $H|m\rangle = E_m|m\rangle$ and $\varrho|m\rangle = \varrho_m|m\rangle$. Then

$$\chi^{\text{ret}}(z) = -i \int_0^\infty dt \, e^{izt} \text{Tr}\varrho[A(t)_H A^\dagger - A^\dagger A(t)_H] \quad (C1)$$

$$= -i \sum_{m,l} \int_0^\infty dt \, e^{i(z+E_m-E_l)t}(\varrho_m - \varrho_l)A_{ml}A_{lm}^\dagger \quad (C2)$$

$$= \sum_{m,l} \frac{\varrho_m - \varrho_l}{z + E_m - E_l}A_{ml}A_{lm}^\dagger. \quad (C3)$$

In the last step, the integral converges for z from the open upper half plane, where $\chi^{\text{ret}}(z)$ is thus analytic.

In this context we remark that the advanced exciton propagator

$$\chi^{\text{adv}}(z) = \int_{-\infty}^\infty dt \, e^{izt}\chi^{\text{adv}}(t), \quad (C4)$$

$$\chi^{\text{adv}}(t) = i\Theta(-t)\langle[A(t)_H, A^\dagger]\rangle \quad (C5)$$

satisfies $\chi^{\text{adv}}(z) = \chi^{\text{ret}}(z^*)^*$ and is analytic in the open lower half plane of z. Its Lehmann representation is formally identical to that of $\chi^{\text{ret}}(z)$ but is obtained from an integral that converges only for z from the open lower half plane.

The Lehmann representation of $\chi_\beta^{\text{Mat}}(\tau)$ in the case $\tau > 0$ is given by

$$\chi_\beta^{\text{Mat}}(\tau) = -\sum_{m,l} \frac{e^{-\beta E_m}}{Z}e^{\tau(E_m-E_l)}A_{ml}A_{lm}^\dagger, \quad \tau > 0. \quad (C6)$$

For $\chi_\beta^{\text{Mat}}(iX_n)$ follows

$$\chi_\beta^{\text{Mat}}(iX_n) = \frac{1}{Z}\sum_{m,l} \frac{e^{-\beta E_m} - e^{-\beta E_l}}{iX_n + E_m - E_l}A_{ml}A_{lm}^\dagger, \quad (C7)$$

by straightforward integration and the use of $e^{i\beta X_n} = 1$. This coincides formally with the Lehmann representation of χ_β^{ret}

and $\chi_\beta^{\mathrm{adv}}$ [compare Eq. (C3)]. However, $\chi_\beta^{\mathrm{Mat}}(z)$ is not defined on the upper or lower half plane of z but only for the Matsubara frequencies $z = iX_n$ on the imaginary z axis.

Next we consider $\chi_\beta^{\mathrm{Mat}}$ in the limit of vanishing temperature. First we study the case $\epsilon_{\mathrm{d}} < \epsilon_{\mathrm{d}0}$, in which $|\Psi_0\rangle$ is the ground state. Due to $e^{-\beta E_m}/Z \to \delta_{m,\Psi_0}$ for $\beta \to \infty$, the Lehmann representation of $\chi_\beta^{\mathrm{Mat}}(\tau)$ approaches

$$\chi_\infty^{\mathrm{Mat}}(\tau) = -\Theta(\tau) \sum_l e^{\tau(E_0 - E_l)} A_{\Psi_0 l} A_{l\Psi_0}^\dagger. \qquad \text{(C8)}$$

Here, $A_{l\Psi_0}^\dagger$ allows only for states l with empty deep level, such that $E_l \geqslant \bar{E}_0 > E_0$. This means that all addends to $\chi_\infty^{\mathrm{Mat}}(\tau)$ decay as $e^{-\tau(\bar{E}_0 - E_0)}$ or faster for $\tau \to \infty$. Therefore,

$$\chi_\infty^{\mathrm{Mat}}(z) = \int_0^\infty d\tau \, e^{z\tau} \chi_\infty^{\mathrm{Mat}}(\tau) \qquad \text{(C9)}$$

$$= \sum_l \frac{1}{z + E_0 - E_l} A_{\Psi_0 l} A_{l\Psi_0}^\dagger \qquad \text{(C10)}$$

constitutes a convergent integral for all z with $\mathrm{Re}\, z < \bar{E}_0 - E_0 \, (> 0)$.

The very same expression results for $\chi_\beta^{\mathrm{ret}}(z) \to \chi_{\Psi_0}^{\mathrm{ret}}(z) = \chi_{\Psi_0}(z)$ from Eq. (C3) in the limit $\beta \to \infty$, in which $\varrho_m \to \delta_{m\Psi_0}$. The two functions thus coincide on the intersection of their domains given by $\mathrm{Re}\, z < \bar{E}_0 - E_0$ and $\mathrm{Im}\, z > 0$ (see Fig. 1).

If instead $\epsilon_{\mathrm{d}} > \epsilon_{\mathrm{d}0}$ such that $|\bar{\Psi}_0\rangle$ is the ground state, the Lehmann representation of $\chi_\beta^{\mathrm{Mat}}(\tau)$ approaches

$$\chi_\infty^{\mathrm{Mat}}(\tau) = -\Theta(-\tau) \sum_m e^{\tau(E_m - \bar{E}_0)} A_{m\bar{\Psi}_0} A_{\bar{\Psi}_0 m}^\dagger \qquad \text{(C11)}$$

for $\beta \to \infty$. For $\tau \to -\infty$ the addends to $\chi^{\mathrm{Mat}}(\tau)$ decay as $e^{\tau(E_0 - \bar{E}_0)}$ or faster. Therefore,

$$\chi_\infty^{\mathrm{Mat}}(z) = \int_{-\infty}^0 d\tau \, e^{z\tau} \chi_\infty^{\mathrm{Mat}}(\tau) \qquad \text{(C12)}$$

$$= \sum_m \frac{-1}{z + E_m - \bar{E}_0} A_{m\bar{\Psi}_0} A_{\bar{\Psi}_0 m}^\dagger \qquad \text{(C13)}$$

constitutes a convergent integral for all z with $\mathrm{Re}\, z > \bar{E}_0 - E_0 \, (< 0)$. We remark in passing that the integration from $-\infty$ to 0 in Eq. (C12) results as the limit of the integration from $-\beta$ to 0. In fact, it is possible to use this interval of integration in Eq. (26) instead of the one from 0 to β, due to $\chi_\beta^{\mathrm{Mat}}(\tau - \beta) = \chi_\beta^{\mathrm{Mat}}(\tau)$ for $0 < \tau < \beta$ and due to $e^{iX_n \beta} = 1$.

The very same expression as for $\chi_\infty^{\mathrm{Mat}}(z)$ in Eq. (C13) results for $\chi_\beta^{\mathrm{adv}}(z)$ in the limit $\beta \to \infty$ with $\varrho_m \to \delta_{m\bar{\Psi}_0}$. In this limit, $\chi_\beta^{\mathrm{adv}}(z)$ converges to

$$\chi_{\bar{\Psi}_0}^{\mathrm{adv}}(z) = \int_{-\infty}^\infty dt \, e^{izt} \chi_{\bar{\Psi}_0}^{\mathrm{adv}}(t) \qquad \text{(C14)}$$

with

$$\chi_{\bar{\Psi}_0}^{\mathrm{adv}}(t) = i\Theta(-t)\langle\bar{\Psi}_0|[A(t)_H, A^\dagger]|\bar{\Psi}_0\rangle. \qquad \text{(C15)}$$

Due to $A^\dagger|\bar{\Psi}_0\rangle = 0$ the advanced exciton propagator $\chi_{\bar{\Psi}_0}^{\mathrm{adv}}$ is in turn identical to the time-ordered propagator in the state $|\bar{\Psi}_0\rangle$:

$$\chi_{\bar{\Psi}_0}^{\mathrm{adv}}(t) = -i\langle\bar{\Psi}_0|\mathcal{T}A(t)_H A^\dagger|\bar{\Psi}_0\rangle = \chi_{\bar{\Psi}_0}(t). \qquad \text{(C16)}$$
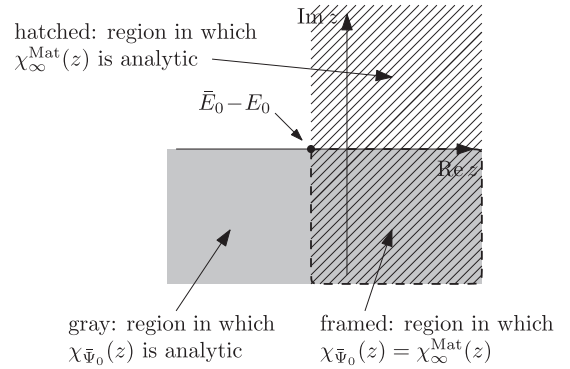

FIG. 4. Domains of analyticity of $\chi_\infty^{\mathrm{Mat}}(z)$ from Eq. (C12) and $\chi_{\Psi_0}(z) = \chi_{\bar{\Psi}_0}^{\mathrm{adv}}(z)$ from Eq. (C14) in the case $\epsilon_{\mathrm{d}} > \epsilon_{\mathrm{d}0}$ in which $|\bar{\Psi}_0\rangle$ is the ground state.

The two functions $\chi_\infty^{\mathrm{Mat}}(z)$ and $\chi_{\bar{\Psi}_0}(z)$ thus coincide on the intersection of their domains given by $\mathrm{Re}\, z > \bar{E}_0 - E_0$ and $\mathrm{Im}\, z < 0$. This relation between $\chi_\infty^{\mathrm{Mat}}(z)$ and $\chi_{\bar{\Psi}_0}(z)$ is sketched in Fig. 4.

APPENDIX D: IDENTITY BETWEEN MATSUBARA DIAGRAMS WITH LIMIT PROPAGATORS AND DIAGRAMS FROM ZERO-TEMPERATURE FORMALISM

In Secs. III D and III E we affirmed that any Matsubara diagram for the particle-hole susceptibility that is evaluated by using the zero-temperature limit propagator from Eq. (44) or (45) is equal to the analytic continuation of the very same diagram evaluated in the zero-temperature formalism. This is shown in the following by using propagators in time representation. We expect that the result holds as well when the diagrams are evaluated with propagators in frequency representation.

Let $D_{\mathrm{lp}}^{\mathrm{Mat}}(\tau)$ denote some time-dependent diagram with n interaction vertices that contributes to the particle-hole susceptibility. As the index "lp" indicates, the diagram is evaluated with limit propagators [in contrast to diagrams $D_\infty^{\mathrm{Mat}}(\tau) = \lim_{\beta \to \infty} D_\beta^{\mathrm{Mat}}(\tau)$ which are evaluated with finite-temperature propagators, the limit $\beta \to \infty$ being taken afterwards]. To each vertex in $D_{\mathrm{lp}}^{\mathrm{Mat}}(\tau)$ is attached an incoming and an outgoing deep-state line as well as an incoming and an outgoing conduction-state line, the lines representing Hartree dressed limit propagators. In total there are $(n + 1)$ deep-state lines and $(n + 1)$ conduction-state lines. Since the deep-state lines $G_{\infty,\mathrm{d}}^{\mathrm{Mat}}(\tau) = e^{-\tilde{\epsilon}_{\mathrm{d}}\tau}\Theta(-\tau)$ are directed backwards in imaginary time they are concatenated in a single sequence from τ to 0, connecting the vertices in a unique time order. Accordingly, we choose the time labels τ_j of the vertices such that $\tau \geqslant \tau_n \geqslant \cdots \geqslant \tau_1 \geqslant 0$. Then the product of all deep-state propagators is

$$e^{-\tilde{\epsilon}_{\mathrm{d}}(\tau_n - \tau)} e^{-\tilde{\epsilon}_{\mathrm{d}}(\tau_{n-1} - \tau_n)} \dots e^{-\tilde{\epsilon}_{\mathrm{d}}(\tau_1 - \tau_2)} e^{-\tilde{\epsilon}_{\mathrm{d}}(0 - \tau_1)} = e^{\tilde{\epsilon}_{\mathrm{d}}\tau}. \qquad \text{(D1)}$$

The vertices are connected in some way by the conduction-state lines. Due to the unique time order of the vertices, the conduction-state lines can be grouped into lines of hole propagation with $\tilde{\epsilon}_k < 0$ and lines of particle propagation with $\tilde{\epsilon}_k > 0$. Let n_{h} be the number of conduction-state hole propagators. The product of all conduction-state lines is then
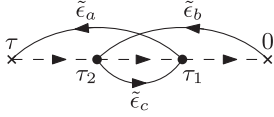
FIG. 5. Example for a diagram $D_{\text{lp}}^{\text{Mat}}(\tau)$ of order $n = 2$. The (Hartree renormalized) energies of the conduction-state lines are $\tilde{\epsilon}_a > 0$, $\tilde{\epsilon}_b > 0$, and $\tilde{\epsilon}_c < 0$ and are addressed as $\tilde{\epsilon}^{\text{in}} = \tilde{\epsilon}_1^{\text{out}} = \tilde{\epsilon}_a$, $\tilde{\epsilon}_1^{\text{in}} = \tilde{\epsilon}_2^{\text{out}} = \tilde{\epsilon}_c$, $\tilde{\epsilon}_2^{\text{in}} = \tilde{\epsilon}_b$.

given by

$$(-1)^{n+1}(-1)^{n_{\text{h}}} e^{-\tau \tilde{\epsilon}^{\text{in}}} e^{-\tau_n(\tilde{\epsilon}_n^{\text{in}} - \tilde{\epsilon}_n^{\text{out}})} \cdots e^{-\tau_1(\tilde{\epsilon}_1^{\text{in}} - \tilde{\epsilon}_1^{\text{out}})}, \qquad \text{(D2)}$$

where $\tilde{\epsilon}_j^{\text{in}}$ and $\tilde{\epsilon}_j^{\text{out}}$ denote the (Hartree renormalized) energy $\tilde{\epsilon}$ of that conduction-state propagator which enters or leaves, respectively, the vertex with time τ_j. Furthermore, $\tilde{\epsilon}^{\text{in}}$ denotes the energy of the conduction-state propagator ending at time τ. An example for this labeling is given in Fig. 5.

The frequency dependence of the diagram is thus given by

$$D_{\text{lp}}^{\text{Mat}}(z) = \frac{1}{V} \int_0^\infty d\tau \, e^{z\tau} (-1)^{n_{\text{loop}}} \left(-\frac{U}{V}\right)^n \int_0^\tau d\tau_n \int_0^{\tau_n} d\tau_{n-1} \cdots \int_0^{\tau_2} d\tau_1 \rho^{n+1} \int_{-\xi_0}^0 d\tilde{\epsilon}_1 \cdots \int_{-\xi_0}^0 d\tilde{\epsilon}_{n_{\text{h}}} \int_0^{\xi_0} d\tilde{\epsilon}_{n_{\text{h}}+1} \cdots \int_0^{\xi_0} d\tilde{\epsilon}_{n+1}$$

$$\times e^{\tilde{\epsilon}_{\text{d}}\tau} (-1)^{n+1}(-1)^{n_{\text{h}}} e^{-\tau \tilde{\epsilon}^{\text{in}}} e^{-\tau_n(\tilde{\epsilon}_n^{\text{in}} - \tilde{\epsilon}_n^{\text{out}})} \cdots e^{-\tau_1(\tilde{\epsilon}_1^{\text{in}} - \tilde{\epsilon}_1^{\text{out}})} \tag{D3}$$

$$= (-1)^{n+1}(-1)^{n_{\text{loop}}} \frac{U^n \rho^{n+1}}{V^{n+1}} \int_{-\xi_0}^0 d\tilde{\epsilon}_1 \cdots \int_{-\xi_0}^0 d\tilde{\epsilon}_{n_{\text{h}}} \int_0^{\xi_0} d\tilde{\epsilon}_{n_{\text{h}}+1} \cdots \int_0^{\xi_0} d\tilde{\epsilon}_{n+1}$$

$$\times \int_0^\infty d\tau \, e^{\tau(z + \tilde{\epsilon}_{\text{d}} - \tilde{\epsilon}^{\text{in}})} \int_0^\tau d\tau_n \, e^{-\tau_n(\tilde{\epsilon}_n^{\text{in}} - \tilde{\epsilon}_n^{\text{out}})} \cdots \int_0^{\tau_2} d\tau_1 \, e^{-\tau_1(\tilde{\epsilon}_1^{\text{in}} - \tilde{\epsilon}_1^{\text{out}})} \tag{D4}$$

[compare Eqs. (27) and (31)]; due to the special role of the deep-state line, the prefactors $(-1)^P/(2^{n_{\text{eq}}}S)$ from Eq. (31) do not arise here. In Eq. (D4), the rightmost integral over imaginary time yields

$$\int_0^{\tau_2} d\tau_1 \, e^{-\tau_1(\tilde{\epsilon}_1^{\text{in}} - \tilde{\epsilon}_1^{\text{out}})} = -\frac{e^{-\tau_2(\tilde{\epsilon}_1^{\text{in}} - \tilde{\epsilon}_1^{\text{out}})} - 1}{\tilde{\epsilon}_1^{\text{in}} - \tilde{\epsilon}_1^{\text{out}}}. \tag{D5}$$

This together with the next integral yields

$$(-1)^2 \left[\frac{e^{-\tau_3(\tilde{\epsilon}_2^{\text{in}} - \tilde{\epsilon}_2^{\text{out}} + \tilde{\epsilon}_1^{\text{in}} - \tilde{\epsilon}_1^{\text{out}})} - 1}{\tilde{\epsilon}_2^{\text{in}} - \tilde{\epsilon}_2^{\text{out}} + \tilde{\epsilon}_1^{\text{in}} - \tilde{\epsilon}_1^{\text{out}}} - \frac{e^{-\tau_3(\tilde{\epsilon}_2^{\text{in}} - \tilde{\epsilon}_2^{\text{out}})} - 1}{\tilde{\epsilon}_2^{\text{in}} - \tilde{\epsilon}_2^{\text{out}}} \right] \frac{1}{\tilde{\epsilon}_1^{\text{in}} - \tilde{\epsilon}_1^{\text{out}}}, \tag{D6}$$

and so on. In particular, the first n integrals produce each a prefactor (-1). Finally, the last imaginary-time integral consists of addends that are made of products of energy denominators and integrations of the type

$$\int_0^\infty d\tau \, e^{\tau(z + \tilde{\epsilon}_{\text{d}} + E)} = \left. \frac{e^{\tau(z + \tilde{\epsilon}_{\text{d}} + E)}}{z + \tilde{\epsilon}_{\text{d}} + E} \right|_0^\infty = -\frac{1}{z + \tilde{\epsilon}_{\text{d}} + E}, \tag{D7}$$

where E is one of

$$-\tilde{\epsilon}^{\text{in}}, \tag{D8}$$

$$-\tilde{\epsilon}^{\text{in}} + \left(\tilde{\epsilon}_n^{\text{out}} - \tilde{\epsilon}_n^{\text{in}}\right), \tag{D9}$$

$$-\tilde{\epsilon}^{\text{in}} + \left(\tilde{\epsilon}_n^{\text{out}} - \tilde{\epsilon}_n^{\text{in}}\right) + \left(\tilde{\epsilon}_{n-1}^{\text{out}} - \tilde{\epsilon}_{n-1}^{\text{in}}\right), \tag{D10}$$

$$\vdots$$

$$-\tilde{\epsilon}^{\text{in}} + \left(\tilde{\epsilon}_n^{\text{out}} - \tilde{\epsilon}_n^{\text{in}}\right) + \left(\tilde{\epsilon}_{n-1}^{\text{out}} - \tilde{\epsilon}_{n-1}^{\text{in}}\right) + \cdots + \left(\tilde{\epsilon}_1^{\text{out}} - \tilde{\epsilon}_1^{\text{in}}\right). \tag{D11}$$

The integral in Eq. (D7) converges for $\text{Re}\,z < -\tilde{\epsilon}_{\text{d}}$, as discussed below. This last integral produces again a prefactor (-1). The combined prefactor $(-1)^{n+1}$ from the time integrals can be merged with the other prefactors to yield

$$D_{\text{lp}}^{\text{Mat}}(z) = (-1)^{n+n_{\text{h}}}(-1)^{n_{\text{loop}}} \frac{U^n \rho^{n+1}}{V^{n+1}} \int_{-\xi_0}^0 d\tilde{\epsilon}_1 \cdots \int_{-\xi_0}^0 d\tilde{\epsilon}_{n_{\text{h}}} \int_0^{\xi_0} d\tilde{\epsilon}_{n_{\text{h}}+1} \cdots \int_0^{\xi_0} d\tilde{\epsilon}_{n+1} \sum_j \frac{1}{z + \tilde{\epsilon}_{\text{d}} + E_j} \cdots \frac{1}{\tilde{\epsilon}_1^{\text{in}} - \tilde{\epsilon}_1^{\text{out}}} \tag{D12}$$

as analytic function on the region given by $\text{Re}\,z < -\tilde{\epsilon}_{\text{d}}$. The sum on the very right of this expression runs over all resulting combinations j of factors. The $(n-1)$ inner factors represented by the dots close to the end of Eq. (D12) may

carry additional sign factors depending on their precise provenance from the inner time integrations [compare Eq. (D6)].

In order to scrutinize the convergence of the outermost imaginary-time integration from Eq. (D7), consider the
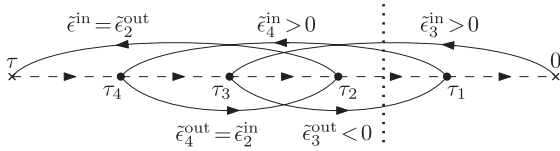
FIG. 6. Example for a diagram $D_{\mathrm{lp}}^{\mathrm{Mat}}(\tau)$ of order $n = 4$ and for the case $m = 2$. The dotted vertical line separates the block of (internal and external) vertices with times $\tau, \tau_n, \ldots, \tau_{n-m}$ from the block with times $\tau_{n-m-1}, \ldots, \tau_1, 0$.

general case

$$
\begin{aligned}
E = {} & -\tilde{\epsilon}^{\mathrm{in}} + \left(\tilde{\epsilon}_n^{\mathrm{out}} - \tilde{\epsilon}_n^{\mathrm{in}}\right) + \left(\tilde{\epsilon}_{n-1}^{\mathrm{out}} - \tilde{\epsilon}_{n-1}^{\mathrm{in}}\right) + \ldots \\
& + \left(\tilde{\epsilon}_{n-m}^{\mathrm{out}} - \tilde{\epsilon}_{n-m}^{\mathrm{in}}\right).
\end{aligned} \tag{D13}
$$

On the right-hand side of this equation, the energies of all conduction-state lines connecting the vertices at times $\tau, \tau_n, \ldots, \tau_{n-m}$ among each other cancel out, as they appear once as some $\tilde{\epsilon}_i^{\mathrm{in}}$ and once as some $\tilde{\epsilon}_j^{\mathrm{out}}$ (see Fig. 6 for an example). There remains the sum of the energies of conduction-state lines connecting the block of vertices at times $\tau, \tau_n, \ldots, \tau_{n-m}$ with the block of vertices at times $\tau_{n-m-1}, \ldots, \tau_1, 0$. If such a line is directed from the former block to the latter one, then it is a hole line with negative energy which enters E as some $\tilde{\epsilon}_j^{\mathrm{out}}$. If the line runs in the opposite direction, then it is a particle line with positive energy

which enters E as some $-\tilde{\epsilon}_j^{\mathrm{in}}$. Consequently, $E \leqslant 0$. This means that the convergence of the integral in Eq. (D7) is guaranteed if $\mathrm{Re}\, z < -\tilde{\epsilon}_{\mathrm{d}}$.

We note that the resulting domain of analyticity differs from the domain of analyticity of $\chi_\infty^{\mathrm{Mat}}(z)$ which is given by $\mathrm{Re}\, z < \bar{E}_0 - E_0 \,(= \epsilon_{\mathrm{d}0} - \epsilon_{\mathrm{d}} = \tilde{\epsilon}_{\mathrm{d}0} - \tilde{\epsilon}_{\mathrm{d}})$ for $\epsilon_{\mathrm{d}} < \epsilon_{\mathrm{d}0}$ and by $\mathrm{Re}\, z > \bar{E}_0 - E_0$ for $\epsilon_{\mathrm{d}} > \epsilon_{\mathrm{d}0}$ (see Sec. II C and Appendix C). This discrepancy highlights that there are diagrams (those with self-energy type insertions on the lines) for which the transition to limit propagators is not correct.

Now we switch from imaginary times to real times and consider the diagram as a contribution to $\chi_{\Psi_0}(z)$ in the state $|\Psi_0\rangle$ as determined by the real-time zero-temperature formalism. We will find the same diagram value on the overlap of the corresponding domains. The Hartree dressed zero-temperature propagators are given by

$$
G(t) = i e^{-i\tilde{\epsilon}t}[\Theta(-\tilde{\epsilon}) - \Theta(t)]. \tag{D14}
$$

Here, the exponent $-i\tilde{\epsilon}t$ is understood as limit of $-i(1 - i\eta)\tilde{\epsilon}t$ for $\eta \to 0^+$ (compare Ref. [4]). Again, the deep-state propagator is directed backwards in time, establishing a unique time order of the vertices with $t \geqslant t_n \geqslant \cdots \geqslant t_1 \geqslant 0$. Similar to the Matsubara case above, the product of all deep-state lines is $i^{n+1} e^{i\tilde{\epsilon}_{\mathrm{d}}t}$, and the product of all conduction-state lines is

$$
(-i)^{n+1}(-1)^{n_{\mathrm{h}}} e^{-it\tilde{\epsilon}^{\mathrm{in}}} e^{-it_n(\tilde{\epsilon}_n^{\mathrm{in}} - \tilde{\epsilon}_n^{\mathrm{out}})} \cdots e^{-it_1(\tilde{\epsilon}_1^{\mathrm{in}} - \tilde{\epsilon}_1^{\mathrm{out}})}. \tag{D15}
$$

The contribution of the diagram to $\chi_{\Psi_0}(z)$ thus turns out to be

$$
\begin{aligned}
D_{\Psi_0}(z) = {} & i^{n+1}(-1)^{n_{\mathrm{h}}+1}(-1)^{n_{\mathrm{loop}}} \frac{U^n \rho^{n+1}}{V^{n+1}} \int_{-\xi_0}^0 d\tilde{\epsilon}_1 \cdots \int_{-\xi_0}^0 d\tilde{\epsilon}_{n_{\mathrm{h}}} \int_0^{\xi_0} d\tilde{\epsilon}_{n_{\mathrm{h}}+1} \cdots \int_0^{\xi_0} d\tilde{\epsilon}_{n+1} \\
& \times \int_0^\infty dt\, e^{it(z+\tilde{\epsilon}_{\mathrm{d}} - \tilde{\epsilon}^{\mathrm{in}})} \int_0^t dt_n\, e^{-it_n(\tilde{\epsilon}_n^{\mathrm{in}} - \tilde{\epsilon}_n^{\mathrm{out}})} \cdots \int_0^{t_2} dt_1\, e^{-it_1(\tilde{\epsilon}_1^{\mathrm{in}} - \tilde{\epsilon}_1^{\mathrm{out}})}.
\end{aligned} \tag{D16}
$$

The real-time integrations at the end of this expression yield precisely the same results as the corresponding imaginary-time integrations in Eqs. (D5)–(D7) above, with the single exception that the prefactor (-1) resulting from every integral is replaced by a factor i. The combined factor i^{n+1} can be merged with the other prefactors to yield for $D_{\Psi_0}(z)$ the identical expression as indicated for $D_{\mathrm{lp}}^{\mathrm{Mat}}(z)$ in Eq. (D12). In the case of $D_{\Psi_0}(z)$, the final time integration decays into addends of the type

$$
\int_0^\infty dt\, e^{it(z+\tilde{\epsilon}_{\mathrm{d}}+E)}, \tag{D17}
$$

which converge for z from the upper half plane, as opposed to the condition $\mathrm{Re}\, z < -\tilde{\epsilon}_{\mathrm{d}}$ for $D_{\mathrm{lp}}^{\mathrm{Mat}}(z)$. On the quadrant allowed by both conditions, the values are identical. This allows for an analytic continuation from the limit-propagator Matsubara diagram to the one from the zero-temperature formalism.

APPENDIX E: ILLUSTRATION OF THE IDENTITY BETWEEN $\chi_\infty^{\mathrm{Mat}}(iX)$ AND $\chi_{\Psi_0}(X)$

In order to illustrate the remarkable equality between the leading-logarithmic approximations for $\chi_\infty^{\mathrm{Mat}}(iX)$ and $\chi_{\Psi_0}(X)$ that was described in Sec. IV B, we refer to the simple ex-

ample of the noninteracting particle-hole susceptibility and the corresponding distribution of poles in the complex plane. The noninteracting particle-hole susceptibility is given in the real-time zero-temperature formalism by

$$
\chi_{\Psi_0}^{\mathrm{nonint}}(z) = -i \frac{\rho}{V} \int_{-\xi_0}^{\xi_0} d\tilde{\epsilon} \int_{-\infty}^\infty \frac{d\omega}{2\pi} \frac{1}{\omega - z - i\eta} \frac{1}{\omega - \tilde{\epsilon} + i\eta\, \mathrm{sgn}\tilde{\epsilon}}. \tag{E1}
$$

The contour of ω integration and the poles of the integrand in the complex ω plane are shown in Fig. 7(a), with z chosen in the open upper left quadrant. The integration contour can now be rotated: The integral along the negative real ω axis is identical to the integral along the negative imaginary ω axis as there are no nonanalyticities in the lower left quadrant and as the integrand decays as $1/\omega^2$ for $|\omega| \to \infty$. Due to the same reasons, the integral along the positive real ω axis equals the integral along the positive imaginary ω axis. With $\omega = i\omega'$ we thus obtain

$$
\chi_{\Psi_0}^{\mathrm{nonint}}(z) = \frac{\rho}{V} \int_{-\xi_0}^{\xi_0} d\tilde{\epsilon} \int_{-\infty}^\infty \frac{d\omega'}{2\pi} \frac{1}{i\omega' - z} \frac{1}{i\omega' - \tilde{\epsilon}} \tag{E2}
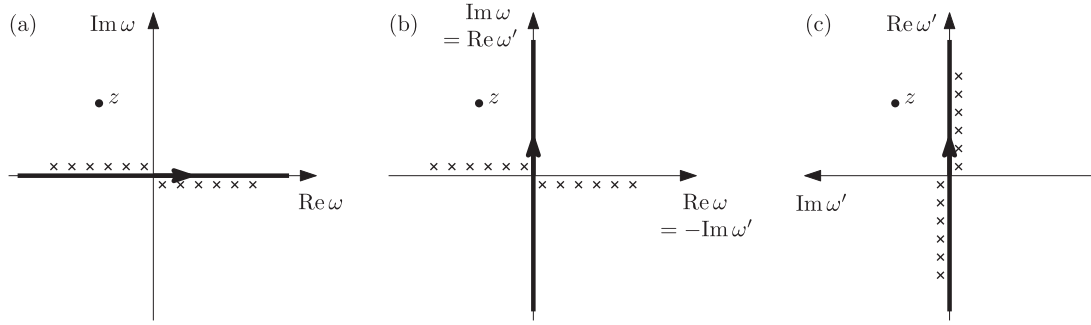$$

$$
= \chi_\infty^{\mathrm{Mat,\, nonint}}(z). \tag{E3}
$$

FIG. 7. (a) Integration contour and poles of the integrand in Eq. (E1). The crosses symbolize the numerous poles at $\tilde{\epsilon}_k - i\eta \, \mathrm{sgn}\tilde{\epsilon}_k$ stemming from the conduction band. (b) Rotated integration contour and the poles of the integrand in Eq. (E2). (c) Integration contour and the poles of the integrand in Eq. (E7).

The infinitesimal shifts $\pm i\eta$ can be omitted once the integration is along the imaginary axis. The new integration contour is shown in Fig. 7(b).

So far we rederived the analytic continuation between χ_{Ψ_0} and $\chi_\infty^{\mathrm{Mat}}$ for the noninteracting case. But now we rewrite $\chi_\infty^{\mathrm{Mat, \, nonint}}(z)$ as

$$\chi_\infty^{\mathrm{Mat, \, nonint}}(z) = -i \int_{-\infty}^{\infty} \frac{d\omega'}{2\pi} \frac{1}{\omega' - (-iz)} \frac{\rho}{V} \int_{-\xi_0}^{\xi_0} \frac{d\tilde{\epsilon}}{i\omega' - \tilde{\epsilon}}$$

(E4)

and use

$$\frac{\rho}{V} \int_{-\xi_0}^{\xi_0} \frac{d\tilde{\epsilon}}{i\omega' - \tilde{\epsilon}} \approx -i\pi \frac{\rho}{V} \mathrm{sgn}(\omega') \Theta(\xi_0 - |\omega'|) \quad (\mathrm{E5})$$

$$\approx \frac{\rho}{V} \int_{-\xi_0}^{\xi_0} \frac{d\tilde{\epsilon}}{\omega' - \tilde{\epsilon} + i\eta \, \mathrm{sgn}\tilde{\epsilon}}. \quad (\mathrm{E6})$$

Here, the first approximation is precisely Eq. (52); the second one is known from Ref. [3] to respect the leading-logarithmic contributions to χ_{Ψ_0}. We obtain

$$\chi_\infty^{\mathrm{Mat, \, nonint}}(z)$$

$$\approx -i\frac{\rho}{V} \int_{-\xi_0}^{\xi_0} d\tilde{\epsilon} \int_{-\infty}^{\infty} \frac{d\omega'}{2\pi} \frac{1}{\omega' - (-iz) - i\eta} \frac{1}{\omega' - \tilde{\epsilon} + i\eta \, \mathrm{sgn}\tilde{\epsilon}}$$

(E7)

$$= \chi_{\Psi_0}^{\mathrm{nonint}}(-iz)$$

(E8)

and in particular $\chi_\infty^{\mathrm{Mat, \, nonint}}(iX) \approx \chi_{\Psi_0}^{\mathrm{nonint}}(X)$. We note that for z from the open upper left quadrant we could simply reintroduce the infinitesimal shift $(-i\eta)$. The poles of the complex integrand are shown in Fig. 7(c). In comparison to Fig. 7(a) it becomes apparent that the main effect of Eq. (E5), i.e., of approximation (52), is to reestablish the pole structure of the conduction-electron states as known from the real-time zero-temperature formalism in a coordinate system with interchanged real- and imaginary-frequency axes.

[1] A. A. Abrikosov, Electron scattering on magnetic impurities in metals and anomalous resistivity effects, Phys. Phys. Fiz. **2**, 5 (1965).

[2] Y. A. Bychkov, L. P. Gor'kov, and I. E. Dzyaloshinskii, Possibility of superconductivity type phenomena in a one-dimensional system, Zh. Eksp. Teor. Fiz. **50**, 738 (1966) [Sov. Phys. JETP **23**, 489 (1966)].

[3] B. Roulet, J. Gavoret, and P. Nozières, Singularities in the x-ray absorption and emission of metals. I. First-order parquet calculation, Phys. Rev. **178**, 1072 (1969).

[4] J. Diekmann and S. G. Jakobs, Parquet approximation and one-loop renormalization group: Equivalence on the leading-logarithmic level, Phys. Rev. B **103**, 155156 (2021).

[5] P. W. Anderson, A poor man's derivation of scaling laws for the Kondo problem, J. Phys. C: Solid State Phys. **3**, 2436 (1970).

[6] J. Sólyom, Renormalization and scaling in the x-ray absorption and Kondo problems, J. Phys. F: Met. Phys. **4**, 2269 (1974).

[7] J. Sólyom, The Fermi gas model of one-dimensional conductors, Adv. Phys. **28**, 201 (1979).

[8] C. Bourbonnais and L. G. Caron, Renormalization group approach to quasi-one-dimensional conductors, Int. J. Mod. Phys. B **5**, 1033 (1991).

[9] W. Metzner, M. Salmhofer, C. Honerkamp, V. Meden, and K. Schönhammer, Functional renormalization group approach to correlated fermion systems, Rev. Mod. Phys. **84**, 299 (2012).

[10] P. Kopietz, L. Bartosch, and F. Schütz, *Introduction to the Functional Renormalization Group*, Lecture Notes in Physics, Vol. 798 (Springer, Berlin, 2010).

[11] C. Platt, W. Hanke, and R. Thomale, Functional renormalization group for multi-orbital Fermi surface instabilities, Adv. Phys. **62**, 453 (2013).

[12] M. Salmhofer, Renormalization in condensed matter: Fermionic systems – from mathematics to materials, Nucl. Phys. B **941**, 868 (2019).

[13] N. Dupuis, L. Canet, A. Eichhorn, W. Metzner, J. M. Pawlowski, M. Tissier, and N. Wschebor, The nonperturbative functional renormalization group and its applications, Phys. Rep. **910**, 1 (2021).

[14] S. G. Jakobs, V. Meden, and H. Schoeller, Nonequilibrium functional renormalization group for interacting quantum systems, Phys. Rev. Lett. **99**, 150603 (2007).

[15] F. B. Kugler and J. v. Delft, Fermi-edge singularity and the functional renormalization group, J. Phys.: Condens. Matter **30**, 195501 (2018).

[16] F. B. Kugler and J. von Delft, Multiloop functional renormalization group that sums up all parquet diagrams, Phys. Rev. Lett. **120**, 057403 (2018).

[17] F. B. Kugler and J. von Delft, Multiloop functional renormalization group for general models, Phys. Rev. B **97**, 035162 (2018).

[18] G. Camacho, C. Klöckner, D. M. Kennes, and C. Karrasch, Review of recent developments of the functional renormalization group for systems out of equilibrium, Eur. Phys. J. B **95**, 195 (2022).

[19] V. Meden, W. Metzner, U. Schollwöck, and K. Schönhammer, A single impurity in a Luttinger liquid: How it "cuts" the chain, J. Low Temp. Phys. **126**, 1147 (2002).

[20] C. Karrasch, M. Pletyukhov, L. Borda, and V. Meden, Functional renormalization group study of the interacting resonant level model in and out of equilibrium, Phys. Rev. B **81**, 125122 (2010).

[21] D. M. Kennes and V. Meden, Interacting resonant-level model in nonequilibrium: Finite-temperature effects, Phys. Rev. B **87**, 075130 (2013).

[22] R. Hedden, V. Meden, T. Pruschke, and K. Schönhammer, A functional renormalization group approach to zero-dimensional interacting systems, J. Phys.: Condens. Matter **16**, 5279 (2004).

[23] R. Gezzi, T. Pruschke, and V. Meden, Functional renormalization group for nonequilibrium quantum many-body problems, Phys. Rev. B **75**, 045324 (2007).

[24] C. Karrasch, R. Hedden, R. Peters, T. Pruschke, K. Schönhammer, and V. Meden, A finite-frequency functional renormalization group approach to the single impurity Anderson model, J. Phys.: Condens. Matter **20**, 345205 (2008).

[25] L. Bartosch, H. Freire, J. J. R. Cardenas, and P. Kopietz, A functional renormalization group approach to the Anderson impurity model, J. Phys.: Condens. Matter **21**, 305602 (2009).

[26] A. Isidori, D. Roosen, L. Bartosch, W. Hofstetter, and P. Kopietz, Spectral function of the Anderson impurity model at finite temperatures, Phys. Rev. B **81**, 235120 (2010).

[27] S. G. Jakobs, M. Pletyukhov, and H. Schoeller, Nonequilibrium functional renormalization group with frequency-dependent vertex function: A study of the single-impurity Anderson model, Phys. Rev. B **81**, 195109 (2010).

[28] M. Kinza, J. Ortloff, J. Bauer, and C. Honerkamp, Alternative functional renormalization group approach to the single impurity Anderson model, Phys. Rev. B **87**, 035111 (2013).

[29] S. Streib, A. Isidori, and P. Kopietz, Solution of the Anderson impurity model via the functional renormalization group, Phys. Rev. B **87**, 201107(R) (2013).

[30] J. F. Rentrop, V. Meden, and S. G. Jakobs, Renormalization group flow of the Luttinger-Ward functional: Conserving approximations and application to the Anderson impurity model, Phys. Rev. B **93**, 195160 (2016).

[31] A. Ge, N. Ritz, E. Walter, S. Aguirre, J. von Delft, and F. B. Kugler, Real-frequency quantum field theory applied to the single-impurity Anderson model, arXiv:2307.10791 [Phys. Rev. B (to be published)].

[32] P. W. Anderson, Localized magnetic states in metals, Phys. Rev. **124**, 41 (1961).

[33] J. R. Schrieffer and P. A. Wolff, Relation between the Anderson and Kondo Hamiltonians, Phys. Rev. **149**, 491 (1966).

[34] P. Nozières, J. Gavoret, and B. Roulet, Singularities in the x-ray absorption and emission of metals. II. Self-consistent treatment of divergences, Phys. Rev. **178**, 1084 (1969).

[35] P. Nozières and C. T. De Dominicis, Singularities in the x-ray absorption and emission of metals. III. One-body theory exact solution, Phys. Rev. **178**, 1097 (1969).

[36] P. Lange, C. Drukier, A. Sharma, and P. Kopietz, Summing parquet diagrams using the functional renormalization group: X-ray problem revisited, J. Phys. A: Math. Theor. **48**, 395001 (2015).

[37] J. W. Negele and H. Orland, *Quantum Many-Particle Systems* (Addison-Wesley, Reading, PA, 1988).

[38] W. Kohn and J. M. Luttinger, Ground-state energy of a many-Fermion system, Phys. Rev. **118**, 41 (1960).

[39] J. M. Luttinger and J. C. Ward, Ground-state energy of a many-Fermion system. II, Phys. Rev. **118**, 1417 (1960).

[40] N. E. Bickers, Parquet equations for numerical self-consistent-field theory, Int. J. Mod. Phys. B **5**, 253 (1991).

[41] Y. M. Vilk and A.-M. S. Tremblay, Non-perturbative many-body approach to the Hubbard model and single-particle pseudogap, J. Phys. I **7**, 1309 (1997).

[42] F. B. Kugler and J. v. Delft, Derivation of exact flow equations from the self-consistent parquet relations, New J. Phys. **20**, 123029 (2018).

[43] A. Tagliavini, C. Hille, F. B. Kugler, S. Andergassen, A. Toschi, and C. Honerkamp, Multiloop functional renormalization group for the two-dimensional Hubbard model: Loop convergence of the response functions, SciPost Phys. **6**, 009 (2019).

[44] C. Hille, D. Rohe, C. Honerkamp, and S. Andergassen, Pseudogap opening in the two-dimensional Hubbard model: A functional renormalization group analysis, Phys. Rev. Res. **2**, 033068 (2020).

[45] C. Hille, F. B. Kugler, C. J. Eckhardt, Y.-Y. He, A. Kauch, C. Honerkamp, A. Toschi, and S. Andergassen, Quantitative functional renormalization group description of the two-dimensional Hubbard model, Phys. Rev. Res. **2**, 033372 (2020).

[46] D. Kiese, T. Müller, Y. Iqbal, R. Thomale, and S. Trebst, Multiloop functional renormalization group approach to quantum spin systems, Phys. Rev. Res. **4**, 023185 (2022).

[47] M. K. Ritter, D. Kiese, T. Müller, F. B. Kugler, R. Thomale, S. Trebst, and J. von Delft, Benchmark calculations of multiloop pseudofermion fRG, Eur. Phys. J. B **95**, 102 (2022).

[48] NIST Digital Library of Mathematical Functions, Release 1.1.10 of 2023-06-15, edited by F. W. J. Olver, A. B. Olde Daalhuis, D. W. Lozier, B. I. Schneider, R. F. Boisvert, C. W. Clark, B. R. Miller, B. V. Saunders, H. S. Cohl, and M. A. McClain, https://dlmf.nist.gov/5.